breco-05/03

BAD 2379, version 11

Collaboration-Wide Review

7 June 2011 to 21 June 2011

Primary BAD	2379, version 11 `Updated Measurement of the Branching Fractions of Color-Suppressed Decays B0bar mesons to D(*)0 pi0, eta, omega, and eta_prime and First Measurement of the Polarization for the Decay D*0 omega`
Author list	Prudent, Xavier; Tisserand, Vincent
Review Committee	comm388, members: Cheng, Chih-hsiang; Kim, Peter (chair); Lacker, Heiko M.
Target	Physical Review D
Result type	
Supporting BAD(s)	BAD #1645 `Measurement of the branching fractions of the color-suppressed decays B0->D(*)0h0, with h0 = pi0, eta, omage, eta'`
Changes since preliminary result	
BAIS/CWR Comments	
Institutional Reading Groups	2b. Budker, Tel Aviv, Colorado, Royal Holloway, McGill, MIT, Trieste 3b. UC Santa Barbara, Colorado State, Dortmund, Ohio State, Oregon, IRFU, Warwick

Cover page generated by BAIS on June 7, 2011

BABAR Analysis Document #2379, Version 11
(Monday June 6, 2011)

Branching Fraction Measurements of the Color-Suppressed Decays $\bar{B}^0$ to $D^{(*)0}\pi^0$, $D^{(*)0}\eta$, $D^{(*)0}\omega$, and $D^{(*)0}\eta'$ and Measurement of the Polarization in the Decay $\bar{B}^0 \to D^{*0}\omega$

J. P. Lees, V. Poireau, and V. Tisserand
Laboratoire d'Annecy-le-Vieux de Physique des Particules (LAPP), Université de Savoie, CNRS/IN2P3, F-74941 Annecy-Le-Vieux, France

J. Garra Tico and E. Grauges
Universitat de Barcelona, Facultat de Fisica, Departament ECM, E-08028 Barcelona, Spain

M. Martinelli[ab], D. A. Milanes[a], A. Palano[ab], and M. Pappagallo[ab]
INFN Sezione di Bari[a]; Dipartimento di Fisica, Università di Bari[b], I-70126 Bari, Italy

G. Eigen and B. Stugu
University of Bergen, Institute of Physics, N-5007 Bergen, Norway

D. N. Brown, L. T. Kerth, Yu. G. Kolomensky, and G. Lynch
Lawrence Berkeley National Laboratory and University of California, Berkeley, California 94720, USA

H. Koch and T. Schroeder
Ruhr Universität Bochum, Institut für Experimentalphysik 1, D-44780 Bochum, Germany

D. J. Asgeirsson, C. Hearty, T. S. Mattison, and J. A. McKenna
University of British Columbia, Vancouver, British Columbia, Canada V6T 1Z1

A. Khan
Brunel University, Uxbridge, Middlesex UB8 3PH, United Kingdom

V. E. Blinov, A. R. Buzykaev, V. P. Druzhinin, V. B. Golubev, E. A. Kravchenko, A. P. Onuchin, S. I. Serednyakov, Yu. I. Skovpen, E. P. Solodov, K. Yu. Todyshev, and A. N. Yushkov
Budker Institute of Nuclear Physics, Novosibirsk 630090, Russia

M. Bondioli, D. Kirkby, A. J. Lankford, M. Mandelkern, and D. P. Stoker
University of California at Irvine, Irvine, California 92697, USA

H. Atmacan, J. W. Gary, F. Liu, O. Long, and G. M. Vitug
University of California at Riverside, Riverside, California 92521, USA

C. Campagnari, T. M. Hong, D. Kovalskyi, J. D. Richman, and C. A. West
University of California at Santa Barbara, Santa Barbara, California 93106, USA

A. M. Eisner, J. Kroseberg, W. S. Lockman, A. J. Martinez, T. Schalk, B. A. Schumm, and A. Seiden
University of California at Santa Cruz, Institute for Particle Physics, Santa Cruz, California 95064, USA

C. H. Cheng, D. A. Doll, B. Echenard, K. T. Flood, D. G. Hitlin, P. Ongmongkolkul, F. C. Porter, and A. Y. Rakitin
California Institute of Technology, Pasadena, California 91125, USA

R. Andreassen, M. S. Dubrovin, Z. Huard, B. T. Meadows, M. D. Sokoloff, and L. Sun
University of Cincinnati, Cincinnati, Ohio 45221, USA

P. C. Bloom, W. T. Ford, A. Gaz, M. Nagel, U. Nauenberg, J. G. Smith, and S. R. Wagner
University of Colorado, Boulder, Colorado 80309, USA

R. Ayad* and W. H. Toki
Colorado State University, Fort Collins, Colorado 80523, USA

B. Spaan
Technische Universität Dortmund, Fakultät Physik, D-44221 Dortmund, Germany

M. J. Kobel, X. Prudent, K. R. Schubert, and R. Schwierz
Technische Universität Dresden, Institut für Kern- und Teilchenphysik, D-01062 Dresden, Germany

D. Bernard and M. Verderi
Laboratoire Leprince-Ringuet, Ecole Polytechnique, CNRS/IN2P3, F-91128 Palaiseau, France

P. J. Clark and S. Playfer
University of Edinburgh, Edinburgh EH9 3JZ, United Kingdom

D. Bettoni[a], C. Bozzi[a], R. Calabrese[ab], G. Cibinetto[ab], E. Fioravanti[ab], I. Garzia[ab], E. Luppi[ab], M. Munerato[ab], M. Negrini[ab], L. Piemontese[a], and V. Santoro
INFN Sezione di Ferrara[a]; Dipartimento di Fisica, Università di Ferrara[b], I-44100 Ferrara, Italy

R. Baldini-Ferroli, A. Calcaterra, R. de Sangro, G. Finocchiaro, M. Nicolaci, P. Patteri, I. M. Peruzzi,† M. Piccolo, M. Rama, and A. Zallo
INFN Laboratori Nazionali di Frascati, I-00044 Frascati, Italy

R. Contri[ab], E. Guido[ab], M. Lo Vetere[ab], M. R. Monge[ab], S. Passaggio[a], C. Patrignani[ab], and E. Robutti[a]
INFN Sezione di Genova[a]; Dipartimento di Fisica, Università di Genova[b], I-16146 Genova, Italy

B. Bhuyan and V. Prasad
Indian Institute of Technology Guwahati, Guwahati, Assam, 781 039, India

C. L. Lee and M. Morii
Harvard University, Cambridge, Massachusetts 02138, USA

A. J. Edwards
Harvey Mudd College, Claremont, California 91711

A. Adametz, J. Marks, and U. Uwer
Universität Heidelberg, Physikalisches Institut, Philosophenweg 12, D-69120 Heidelberg, Germany

F. U. Bernlochner, M. Ebert, H. M. Lacker, and T. Lueck
Humboldt-Universität zu Berlin, Institut für Physik, Newtonstr. 15, D-12489 Berlin, Germany

P. D. Dauncey and M. Tibbetts
Imperial College London, London, SW7 2AZ, United Kingdom

P. K. Behera and U. Mallik
University of Iowa, Iowa City, Iowa 52242, USA

C. Chen, J. Cochran, W. T. Meyer, S. Prell, E. I. Rosenberg, and A. E. Rubin
Iowa State University, Ames, Iowa 50011-3160, USA

A. V. Gritsan and Z. J. Guo
Johns Hopkins University, Baltimore, Maryland 21218, USA

N. Arnaud, M. Davier, G. Grosdidier, F. Le Diberder, A. M. Lutz, B. Malaescu, P. Roudeau, M. H. Schune, A. Stocchi, and G. Wormser
Laboratoire de l'Accélérateur Linéaire, IN2P3/CNRS et Université Paris-Sud 11, Centre Scientifique d'Orsay, B. P. 34, F-91898 Orsay Cedex, France

D. J. Lange and D. M. Wright
Lawrence Livermore National Laboratory, Livermore, California 94550, USA

I. Bingham, C. A. Chavez, J. P. Coleman, J. R. Fry, E. Gabathuler, D. E. Hutchcroft, D. J. Payne, and C. Touramanis
University of Liverpool, Liverpool L69 7ZE, United Kingdom

A. J. Bevan, F. Di Lodovico, R. Sacco, and M. Sigamani
Queen Mary, University of London, London, E1 4NS, United Kingdom

G. Cowan
University of London, Royal Holloway and Bedford New College, Egham, Surrey TW20 0EX, United Kingdom

D. N. Brown and C. L. Davis
University of Louisville, Louisville, Kentucky 40292, USA

A. G. Denig, M. Fritsch, W. Gradl, A. Hafner, and E. Prencipe
Johannes Gutenberg-Universität Mainz, Institut für Kernphysik, D-55099 Mainz, Germany

K. E. Alwyn, D. Bailey, R. J. Barlow,[‡] G. Jackson, and G. D. Lafferty
University of Manchester, Manchester M13 9PL, United Kingdom

R. Cenci, B. Hamilton, A. Jawahery, D. A. Roberts, and G. Simi
University of Maryland, College Park, Maryland 20742, USA

C. Dallapiccola
University of Massachusetts, Amherst, Massachusetts 01003, USA

R. Cowan, D. Dujmic, and G. Sciolla
Massachusetts Institute of Technology, Laboratory for Nuclear Science, Cambridge, Massachusetts 02139, USA

D. Lindemann, P. M. Patel, S. H. Robertson, and M. Schram
McGill University, Montréal, Québec, Canada H3A 2T8

P. Biassoni[ab], A. Lazzaro[ab], V. Lombardo[a], N. Neri[ab], F. Palombo[ab], and S. Stracka[ab]
INFN Sezione di Milano[a]; Dipartimento di Fisica, Università di Milano[b], I-20133 Milano, Italy

L. Cremaldi, R. Godang,[§] R. Kroeger, P. Sonnek, and D. J. Summers
University of Mississippi, University, Mississippi 38677, USA

X. Nguyen and P. Taras
Université de Montréal, Physique des Particules, Montréal, Québec, Canada H3C 3J7

G. De Nardo[ab], D. Monorchio[ab], G. Onorato[ab], and C. Sciacca[ab]
INFN Sezione di Napoli[a]; Dipartimento di Scienze Fisiche,
Università di Napoli Federico II[b], I-80126 Napoli, Italy

G. Raven and H. L. Snoek
NIKHEF, National Institute for Nuclear Physics and High Energy Physics, NL-1009 DB Amsterdam, The Netherlands

C. P. Jessop, K. J. Knoepfel, J. M. LoSecco, and W. F. Wang
University of Notre Dame, Notre Dame, Indiana 46556, USA

K. Honscheid and R. Kass
Ohio State University, Columbus, Ohio 43210, USA

J. Brau, R. Frey, N. B. Sinev, D. Strom, and E. Torrence
University of Oregon, Eugene, Oregon 97403, USA

E. Feltresi[ab], N. Gagliardi[ab], M. Margoni[ab], M. Morandin[a],
M. Posocco[a], M. Rotondo[a], F. Simonetto[ab], and R. Stroili[ab]
INFN Sezione di Padova[a]; Dipartimento di Fisica, Università di Padova[b], I-35131 Padova, Italy

E. Ben-Haim, M. Bomben, G. R. Bonneaud, H. Briand, G. Calderini,
J. Chauveau, O. Hamon, Ph. Leruste, G. Marchiori, J. Ocariz, and S. Sitt
Laboratoire de Physique Nucléaire et de Hautes Energies,
IN2P3/CNRS, Université Pierre et Marie Curie-Paris6,
Université Denis Diderot-Paris7, F-75252 Paris, France

M. Biasini[ab], E. Manoni[ab], S. Pacetti[ab], and A. Rossi[ab]
INFN Sezione di Perugia[a]; Dipartimento di Fisica, Università di Perugia[b], I-06100 Perugia, Italy

C. Angelini[ab], G. Batignani[ab], S. Bettarini[ab], M. Carpinelli[ab],[¶] G. Casarosa[ab], A. Cervelli[ab], F. Forti[ab],
M. A. Giorgi[ab], A. Lusiani[ac], B. Oberhof[ab], E. Paoloni[ab], A. Perez[a], G. Rizzo[ab], and J. J. Walsh[a]
INFN Sezione di Pisa[a]; Dipartimento di Fisica, Università di Pisa[b]; Scuola Normale Superiore di Pisa[c], I-56127 Pisa, Italy

D. Lopes Pegna, C. Lu, J. Olsen, A. J. S. Smith, and A. V. Telnov
Princeton University, Princeton, New Jersey 08544, USA

F. Anulli[a], G. Cavoto[a], R. Faccini[ab], F. Ferrarotto[a], F. Ferroni[ab],
M. Gaspero[ab], L. Li Gioi[a], M. A. Mazzoni[a], and G. Piredda[a]
INFN Sezione di Roma[a]; Dipartimento di Fisica,
Università di Roma La Sapienza[b], I-00185 Roma, Italy

C. Bünger, O. Grünberg, T. Hartmann, T. Leddig, H. Schröder, and R. Waldi
Universität Rostock, D-18051 Rostock, Germany

T. Adye, E. O. Olaiya, and F. F. Wilson
Rutherford Appleton Laboratory, Chilton, Didcot, Oxon, OX11 0QX, United Kingdom

S. Emery, G. Hamel de Monchenault, G. Vasseur, and Ch. Yèche
CEA, Irfu, SPP, Centre de Saclay, F-91191 Gif-sur-Yvette, France

D. Aston, D. J. Bard, R. Bartoldus, C. Cartaro, M. R. Convery, J. Dorfan, G. P. Dubois-Felsmann, W. Dunwoodie,
R. C. Field, M. Franco Sevilla, B. G. Fulsom, A. M. Gabareen, M. T. Graham, P. Grenier, C. Hast, W. R. Innes,
M. H. Kelsey, H. Kim, P. Kim, M. L. Kocian, D. W. G. S. Leith, P. Lewis, S. Li, B. Lindquist, S. Luitz, V. Luth,
H. L. Lynch, D. B. MacFarlane, D. R. Muller, H. Neal, S. Nelson, I. Ofte, M. Perl, T. Pulliam, B. N. Ratcliff,
A. Roodman, A. A. Salnikov, R. H. Schindler, A. Snyder, D. Su, M. K. Sullivan, J. Va'vra, A. P. Wagner,
M. Weaver, W. J. Wisniewski, M. Wittgen, D. H. Wright, H. W. Wulsin, A. K. Yarritu, C. C. Young, and V. Ziegler
SLAC National Accelerator Laboratory, Stanford, California 94309 USA

W. Park, M. V. Purohit, R. M. White, and J. R. Wilson
University of South Carolina, Columbia, South Carolina 29208, USA

A. Randle-Conde and S. J. Sekula
Southern Methodist University, Dallas, Texas 75275, USA

M. Bellis, J. F. Benitez, P. R. Burchat, and T. S. Miyashita
Stanford University, Stanford, California 94305-4060, USA

M. S. Alam and J. A. Ernst
State University of New York, Albany, New York 12222, USA

R. Gorodeisky, N. Guttman, D. R. Peimer, and A. Soffer
Tel Aviv University, School of Physics and Astronomy, Tel Aviv, 69978, Israel

P. Lund and S. M. Spanier

University of Tennessee, Knoxville, Tennessee 37996, USA

R. Eckmann, J. L. Ritchie, A. M. Ruland, C. J. Schilling, R. F. Schwitters, and B. C. Wray
University of Texas at Austin, Austin, Texas 78712, USA

J. M. Izen and X. C. Lou
University of Texas at Dallas, Richardson, Texas 75083, USA

F. Bianchi[ab] and D. Gamba[ab]
INFN Sezione di Torino[a]; Dipartimento di Fisica Sperimentale, Università di Torino[b], I-10125 Torino, Italy

L. Lanceri[ab] and L. Vitale[ab]
INFN Sezione di Trieste[a]; Dipartimento di Fisica, Università di Trieste[b], I-34127 Trieste, Italy

F. Martinez-Vidal and A. Oyanguren
IFIC, Universitat de Valencia-CSIC, E-46071 Valencia, Spain

H. Ahmed, J. Albert, Sw. Banerjee, H. H. F. Choi, G. J. King, R. Kowalewski, M. J. Lewczuk, C. Lindsay, I. M. Nugent, J. M. Roney, R. J. Sobie, and N. Tasneem
University of Victoria, Victoria, British Columbia, Canada V8W 3P6

T. J. Gershon, P. F. Harrison, T. E. Latham, and E. M. T. Puccio
Department of Physics, University of Warwick, Coventry CV4 7AL, United Kingdom

H. R. Band, S. Dasu, Y. Pan, R. Prepost, and S. L. Wu
University of Wisconsin, Madison, Wisconsin 53706, USA

(The *BABAR* Collaboration)

(Dated: June 6, 2011)

We report results on the updated branching fraction ($\mathcal{B}$) measurements of the color-suppressed decays $\overline{B}^0 \to D^0\pi^0$, $D^{*0}\pi^0$, $D^0\eta$, $D^{*0}\eta$, $D^0\omega$, $D^{*0}\omega$, $D^0\eta'$, and $D^{*0}\eta'$. We measure the branching fractions $\mathcal{B}(\overline{B}^0 \to D^0\pi^0) = (2.69 \pm 0.09 \pm 0.13) \times 10^{-4}$, $\mathcal{B}(\overline{B}^0 \to D^{*0}\pi^0) = (3.05 \pm 0.14 \pm 0.28) \times 10^{-4}$, $\mathcal{B}(\overline{B}^0 \to D^0\eta) = (2.53 \pm 0.09 \pm 0.11) \times 10^{-4}$, $\mathcal{B}(\overline{B}^0 \to D^{*0}\eta) = (2.69 \pm 0.14 \pm 0.23) \times 10^{-4}$, $\mathcal{B}(\overline{B}^0 \to D^0\omega) = (2.57 \pm 0.11 \pm 0.14) \times 10^{-4}$, $\mathcal{B}(\overline{B}^0 \to D^{*0}\omega) = (4.55 \pm 0.24 \pm 0.39) \times 10^{-4}$, $\mathcal{B}(\overline{B}^0 \to D^0\eta') = (1.48 \pm 0.13 \pm 0.07) \times 10^{-4}$, and $\mathcal{B}(\overline{B}^0 \to D^{*0}\eta') = (1.49 \pm 0.22 \pm 0.15) \times 10^{-4}$. We also present the first measurement of the longitudinal fraction of the channel $D^{*0}\omega$, f_L=$(66.5 \pm 4.7 \pm 1.5)\%$. In the above, the first uncertainty is statistical and the second is systematic. The results are based on a sample of $(454 \pm 5) \times 10^6 B\overline{B}$ pairs collected at the $\Upsilon(4S)$ resonance from 1999 to 2007, with the *BABAR* detector at the PEP-II storage rings at SLAC. The measurements are the most precise determinations of these quantities from a single experiment. They are compared to theoretical predictions obtained by factorization, Soft Collinear Effective Theory (SCET) and perturbative QCD (pQCD). We find that the presence of final state interactions is favored and the measurements are in better agreement with SCET when compared to pQCD.

PACS numbers: 13.25.Hw, 12.15.Hh, 11.30.Er

I. INTRODUCTION

Weak decays of hadrons provide a direct access to the parameters of the Cabibbo-Kobayashi-Maskawa (CKM) matrix and thus to the study of *CP* violation. Strong interaction scattering in the final state [1] (Final State Interactions, or FSI) can modify the decay dynamics and must be well understood. The two-body hadronic decays with a charmed final state, $B \to D^{(*)}h$, where h is a light meson, are of great help in studying strong-interaction physics related to the confinement of quarks and gluons into hadrons.

The decays $B \to D^{(*)}h$ can proceed through the emis-

* Now at Temple University, Philadelphia, Pennsylvania 19122, USA
† Also with Università di Perugia, Dipartimento di Fisica, Perugia, Italy
‡ Now at the University of Huddersfield, Huddersfield HD1 3DH, UK
§ Now at University of South Alabama, Mobile, Alabama 36688, USA
¶ Also with Università di Sassari, Sassari, Italy

sion of a $W^\pm$ boson following three possible diagrams: external, internal (see Fig. 1), or by a $W^\pm$ boson exchange whose contribution is much smaller [2]. The neutral $\overline{B}^0 \to D^{(*)0}h^0$ decays proceed through the internal diagrams [3]. Since mesons are color singlet objects, in internal diagrams $\overline{B}^0 \to D^{(*)0}h^0$ the quarks from the $W^\pm$ decay are constrained to have the anti-color of the spectator quark, which induces a suppression of internal diagrams in comparison with external ones. For this reason, internal diagrams are called *color-suppressed* and external ones are called *color-favored*.

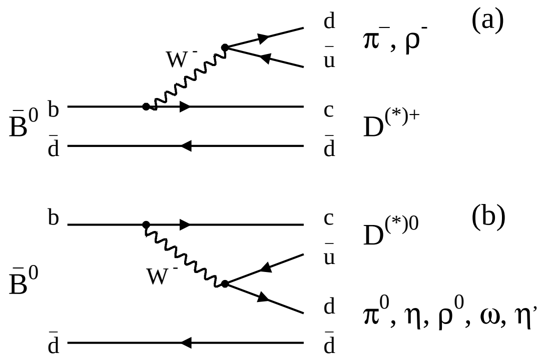

FIG. 1. External (a) and internal (b) tree diagrams for $\overline{B}^0 \to D^{(*)}h$ decays.

In the factorization model [3–6], the non-factorizable interactions in the final state by soft gluons are neglected. The matrix element in the effective weak Hamiltonian of the decay $B \to Dh$ is then factorized into a product of asymptotic states. Factorization appears to be successful in the description of the color-favored decays [7].

The color-suppressed $b \to c$ decays $\overline{B}^0 \to D^{(*)0}\pi^0$ were first observed by the CLEO [8] and Belle [9] collaborations in 2001 with respectively 9.67×10^6 and 23.1×10^6 $B\overline{B}$ pairs. The Belle collaboration has also observed the decays $D^0\eta$ and $D^0\omega$ and put upper limits on the branching fraction ($\mathcal{B}$) of $D^{*0}\eta$ and $D^{*0}\omega$ [9].

The $\mathcal{B}$ of the color-suppressed decays $\overline{B}^0 \to D^{(*)0}\pi^0$, $D^{(*)0}\eta$, $D^{(*)0}\omega$, and $D^0\eta'$ were measured by *BABAR* [10] in 2003 with 88×10^6 $B\overline{B}$ pairs and an upper limit was set on $\mathcal{B}(\overline{B}^0 \to D^{*0}\eta')$. The Belle collaboration updated with 152×10^6 $B\overline{B}$ pairs the measurement of $\mathcal{B}(\overline{B}^0 \to D^{(*)0}h^0)$, $h^0 = \pi^0$, η, ω, and η' [11] in 2005 and [12] in 2006 and studied in 2007 the decays $\overline{B}^0 \to D^0\rho^0$ with 388×10^6 $B\overline{B}$ pairs [13]. In an alternative approach, *BABAR* [14] used the charmless neutral B to $K^\pm\pi^\mp\pi^0$ Dalitz plot analysis with 232×10^6 $B\overline{B}$ pairs, and found $\mathcal{B}(\overline{B}^0 \to D^0\pi^0)$ to be in excellent agreement with earlier experimental results.

Many of these branching fraction measurements are significantly larger than predictions obtained within the factorization approximation [15]. It is also well agreed that non-factorizable contributions are mostly dominant for color-suppressed charmed B decays and therefore can not be neglected [16].

While the initial various experimental results demonstrated overall good consistency, the most recent measurements performed by Belle [11, 12] have shown a tendency to systematically lower $\mathcal{B}$ values for the color-suppressed $\overline{B}^0 \to D^{(*)0}h^0$ decays. Such lower $\mathcal{B}$ measurements are closer to factorization predictions [3, 15].

Stronger experimental constraints are therefore needed to distinguish between the different models of the color-suppressed dynamics like pQCD (*perturbative QCD*) [17, 18] or SCET (*Soft Collinear Effective Theory*) [19–21]. Finally we emphasize again the need of accurate measurements for hadronic color-suppressed $\overline{B}^0 \to D^{(*)0}h^0$ decays for constraining the theoretical predictions on $\bar{B}_{u,d,s}$ decays to $D^{(*)}P$ and $\bar{D}^{(*)}P$ decays, where P is a light pseudoscalar meson such as a pion or a kaon (see for example [22]). These decays are and will be employed to extract the less accurately measured CKM-angle γ and other angles [23], especially at the dawn of the B-physics program at the LHC.

This paper reports the improved branching fraction measurements of eight color-suppressed decays $\overline{B}^0 \to D^{(*)0}\pi^0$, $D^{(*)0}\eta$, $D^{(*)0}\omega$ and $D^{(*)0}\eta'$ with 454×10^6 $B\overline{B}$ pairs and shows for the first time the measurement of the longitudinal polarization for the decay mode into two vector mesons $\overline{B}^0 \to D^{*0}\omega$.

II. THE *BABAR* DETECTOR AND DATA SAMPLE

The data used in this analysis were collected with the *BABAR* detector at the PEP-II asymmetric e^+e^- storage rings operating at the SLAC National Accelerator Laboratory. The *BABAR* detector is described in detail in Ref. [24]. Charged particle tracks are reconstructed using a five-layer silicon vertex tracker (SVT) and a 40-layer drift chamber (DCH) immersed in a 1.5 T magnetic field. Tracks are identified as pions or kaons (particle identification or PID) based on likelihoods constructed from energy loss measurements in the SVT and the DCH and from Cherenkov radiation angles measured in the detector of internally reflected Cherenkov light (DIRC). Photons are reconstructed from showers measured in the CsI(Tl) crystal electromagnetic calorimeter (EMC). Muon and neutral hadron identification are performed with the instrumented flux return (IFR).

The results presented in this paper are based on a data sample of an integrated luminosity of 413 fb^{-1} recorded at the $\Upsilon(4S)$ resonance with a e^+e^- center-of-mass (CM) energy of 10.58 GeV, corresponding to $(454\pm5)\times10^6$ $B\overline{B}$ pairs. As suggested in the Particle Data Group (PDG) mini-review on production and decay of $b-$ flavored hadrons [25], we assume equal $B^0\overline{B}^0$ and B^+B^- production rate at that resonance in this paper. A data sample of 41.2 fb^{-1} with a CM energy of 10.54 GeV, below the $B\overline{B}$ threshold, is used to study background contributions from continuum events $e^+e^- \to q\overline{q}$ ($q = u$, d, s, c). We call that latter data set *off-peak events* in what follows.

Samples of simulated Monte Carlo (MC) events were used to determine signal and background characteristics, to optimize selection criteria and to evaluate efficiencies. Simulated events $e^+e^- \to \Upsilon(4S) \to B^+B^-,\ B^0\overline{B}^0$, $e^+e^- \to q\overline{q}$ ($q = u,\ d,\ s$) and $e^+e^- \to c\overline{c}$ are generated with `EvtGen` [26], which interfaces to `Pythia` [27] and `Jetset` [28].

Separate samples of exclusive $\overline{B}^0 \to D^{(*)0}h^0$ decays were generated to study the signal features and to quantify the signal selection efficiencies. We use high statistics control samples of exclusive decays $B^- \to D^{(*)}\pi^-$ and $D^{(*)0}\rho^-$ for the specific selections and background studies. Those control samples have been generated in the Monte Carlo simulation and similarly selected in the data. All MC samples include simulation of the *BABAR* detector response generated through `Geant4` [29]. The integrated luminosity of the MC samples is about three times the data luminosity for $B\overline{B}$, one times the data luminosity for $e^+e^- \to q\overline{q}$ ($q = u,\ d,\ s$) and two times for $e^+e^- \to c\overline{c}$. The equivalent integrated luminosities of the exclusive B decay mode simulations range from 50 to 2500 times the data luminosity.

III. ANALYSIS METHOD

A. General considerations

The color-suppressed $\overline{B}^0$ meson decay modes are reconstructed from $D^{(*)0}$ meson candidates that are combined with light neutral-meson candidates h^0 (π^0, η, ω, and η'). The $D^{(*)}$ and h^0 mesons are detected in various possible channels. In total, we consider 72 different $\overline{B}^0 \to D^{(*)0}h^0$ decay modes.

We perform a blind analysis: the optimization of the various event selections, the background characterizations and rejections, the efficiency calculations, and most of the systematic uncertainties computations are based on studies done with MC simulations, data sidebands, or data control samples. The fits to data, including the various signal regions, are only effected after all analysis procedures are determined and systematic uncertainties are studied.

Intermediate resonances of the decays $\overline{B}^0 \to D^{(*)0}h^0$ are reconstructed by combining tracks and/or photons for the channels with the highest decay rate and detection efficiency. Vertex constraints are applied to charged daughter particles of these resonances before computing their invariant masses. At each step in the decay chain we require that mesons have masses consistent with their assumed particle type. If daughter particles are produced in the decay of a parent meson with a natural width that is small relative to the reconstructed width (except for ω and ρ^0 mesons), we constrain the meson's mass to its nominal value [25]. This fitting technique improves the resolution of the energy and the momentum of the $\overline{B}^0$ candidates as they are calculated from improved energies and momenta of the $D^{(*)0}$ and h^0.

Charged particle tracks are reconstructed from measurements in the SVT and/or the DCH, and an identification is assigned by the PID algorithm. Extrapolated tracks must be in the vicinity of the e^+e^- interaction point, *i.e.* within 1.5 cm in the plane transverse to the beam axis and 2.5 cm along the beam axis. The tracks used for the reconstruction of $\eta \to \pi^+\pi^-\pi^0$ and $\eta' \to \pi^+\pi^-\eta(\to \gamma\gamma)$ must in addition have a transverse momentum p_T larger than 100 MeV/c and at least 12 hits in the DCH. When PID criterion is required for a track, the track polar angle θ must be in the DIRC fiducial region $25.78^\circ < \theta < 146.10^\circ$. Photons are defined as single bumps in the EMC crystals not matched with any track, and with a shower lateral shape consistent with a photon. Because of high background levels in the very forward part of the EMC caused by the beam asymmetry, we reject photons detected in the region $\theta < 21.19^\circ$.

The selections applied to each meson (π^0, η, ω, η', D^0, and D^{*0}) are optimized by maximizing the figure of merit $S/\sqrt{S+B}$, where S is the number of signal and B is the number of background events. The numbers S and B are computed from simulations, the branching ratios used to evaluate S are the present world average values of color-suppressed decay mode provided by PDG [25]. Each resonance mass distribution is fitted with a set of Gaussian functions or a so-called *modified Novosibirsk* empirical function [30], which is composed of a Gaussian-like peaking part with two tails at low and high values. Resonance candidates are then required to have a mass within $\pm 2.5\sigma$ around the fitted mass central value, where σ is the resolution of the mass distribution obtained by the fit. For the resonances $D^0 \to K^-\pi^+\pi^0$ and $D^{*0} \to D^0\gamma$, the lower bound is extended to -3σ because of the photon energy losses in front and between the EMC crystals, which makes the mass distribution asymmetric with a tail at low values.

B. Selection of intermediate resonances

1. π^0 selection

The π^0 mesons are reconstructed from photon pairs. Each photon energy $E(\gamma)$ must be larger than 85 MeV for π^0 produced directly from B^0 decays, and larger than 60 MeV for π^0 from η, ω or D^0 meson decays. Soft π^0's originating from $D^{*0} \to D^0\pi^0$ decays must satisfy $E(\gamma) > 30$ MeV. The π^0 reconstructed mass resolution is about $6.5 - 7.0$ MeV/c^2 for π^0 from η, ω, and D^0 mesons decays, and about $7.0 - 7.5$ MeV/c^2 for π^0 produced in D^{*0} or B^0 decays.

2. η selection

The η mesons are reconstructed in the $\gamma\gamma$ and $\pi^+\pi^-\pi^0$ decay modes. These modes account for about 62% of the total decay rate [25], and may originate from $\overline{B}^0 \to D^{(*)0}\eta$ or $\eta' \to \pi^+\pi^-\eta$ decays.

The $\eta \to \gamma\gamma$ candidates are reconstructed by combining two photons that satisfy $E(\gamma) > 200$ MeV for $\overline{B}^0$ daughters and $E(\gamma) > 180$ MeV for η' daughters. As photons originating from high momentum π^0 mesons may fake a $\eta \to \gamma\gamma$ signal, a veto is applied against those π^0: for each $\eta \to \gamma\gamma$ candidate, if any of the other photons in the events with $E(\gamma) > 200$ MeV combined with either photon in η has an invariant mass between 115 and 150 MeV/c^2, the η candidate is rejected. Such a veto is highly efficient on signal (about 91−95%) while it reduces the background of fake η mesons candidates by a factor of two. The resolution of the $\eta \to \gamma\gamma$ mass distribution is approximately 15 MeV/c^2, dominated by the resolution on the photon energy measurement in the EMC.

For η candidates reconstructed in the channel $\pi^+\pi^-\pi^0$, the π^0 is required to satisfy the conditions described in Sec. III B 1. The mass resolution is about 3 MeV/c^2, which is smaller than for the mode $\eta \to \gamma\gamma$, thanks to the relatively better resolution of the tracking system and the various vertex and mass constraints applied to the η and π^0 candidates.

3. ω selection

The ω mesons are reconstructed in the $\pi^+\pi^-\pi^0$ decay mode. These modes account for approximately 89% of the total decay rate. The π^0 is required to satisfy the conditions described in Sec. III B 1 and the transverse momentum of the charged pions must be greater than 200 MeV/c. The natural width of the ω mass distribution $\Gamma \sim 8.49$ MeV [25] is comparable to the experimental resolution $\sigma \sim 7$ MeV/c^2, therefore the ω mass is not constrained to its nominal value. We define a total width $\sigma_{tot} = \sqrt{\sigma^2 + \Gamma^2/c^2} \sim 11$ MeV/c^2 and require the ω candidates to satisfy $|m(\omega) - m(\omega)_{\rm mean}| < 2.5\sigma_{tot}$.

4. ρ^0 selection

The ρ^0 mesons originate from $\eta' \to \rho^0\gamma$ and are reconstructed in the $\pi^+\pi^-$ decay mode. The charged tracks must satisfy $p_T(\pi^\pm) > 100$ MeV/c. We define the helicity angle θ_{ρ^0} as the angle between the pion momentum in the ρ^0 rest frame and the ρ^0 momentum in the η' rest frame. Because the ρ^0 meson is a vector meson and the charged pions are pseudo-scalar mesons, the angular distribution is proportional to $\sin^2(\theta_{\rho^0})$ for signal, and is flat for background. The ρ^0 candidates with $|\cos(\theta_{\rho^0})| > 0.73$ are rejected. Due to the large ρ^0 natural width $\Gamma \sim 149.1$ MeV [25], no mass constraint is applied to the ρ^0. The mass of the ρ^0 candidate must be within 160 MeV/c^2 around the nominal mass value and no mass constraint is applied.

5. η' selection

The η' mesons are reconstructed in the $\pi^+\pi^-\eta(\to\gamma\gamma)$ and $\rho^0\gamma$ decay modes. These modes account for approximately 46.3% of the total decay rate.

Only the $\eta \to \gamma\gamma$ sub-mode is used in the $\pi^+\pi^-\eta$ reconstruction due to its higher efficiency. The selection is described in Sec. III B 2. For candidates reconstructed in $\rho^0\gamma$, channel we select ρ^0 as described in Sec. III B 4, and the photons must have an energy larger than 200 MeV. As photons coming from π^0 decays may fake signal, a veto against π^0 as described in Sec. III B 2 is applied. The η' mass resolution is about 3 MeV/c^2 for $\pi^+\pi^-\eta$ and 8 MeV/c^2 for $\rho^0\gamma$.

6. K^0_S selection

The K^0_S mesons are reconstructed through their decay to two charged pions ($\pi^-\pi^+$) which must originate from a common vertex. These modes account for 69% of the total decay rate. The χ^2 probability of the vertex fit of the pair of charged pions must be larger than 0.1%. We define the flight significance as the ratio L/σ_L, where L is the K^0_S flight length in the plane transverse to the beam axis and σ_L is the resolution on L determined from the vertex fit constraint. The combinatorial background is rejected by requiring a flight significance larger than 5. The reconstructed K^0_S mass resolution is about 2 MeV/c^2 for a core Gaussian part corresponding to about 70% of the candidates and 5 MeV/c^2 for the remaining part, depending on the transverse position of the decay of the K^0_S within the tracking system (SVT or DCH).

7. D^0 selection

The D^0 mesons are reconstructed in the $K^-\pi^+$, $K^-\pi^+\pi^0$, $K^-\pi^+\pi^-\pi^+$, and $K^0_S\pi^+\pi^-$ decay modes. These modes account for about 29% of the total decay rate. All D^0 candidates must satisfy $p^*(D^0) > 1.1$ GeV/c, where p^* refers to the value of the momentum computed in the $\Upsilon(4S)$ rest frame. That requirement is loose enough so that various sources of background can populate the sidebands of the signal region.

For the decay modes reconstructed only with tracks, we require that the charged pions originated from the D^0 candidates must fulfill $p_T(\pi^\pm) > 400$ MeV/c for $K^-\pi^+$, $p_T(\pi^\pm) > 100$ MeV/c for $K^-\pi^+\pi^-\pi^+$, and $p_T(\pi^\pm) > 120$ MeV/c for $K^0_S\pi^-\pi^+$. Where p_T is the transverse component to the beam axis of the momentum computed in the laboratory.

The charged tracks must originate from a common vertex, therefore the χ^2 probability of the vertex fit must be larger than 0.1% for the channel $K^-\pi^+$ and larger than 0.5% for the other modes with more abundant background. Because of the increasing level of background present for the various decay modes, the kaon candidates must satisfy from looser to tighter PID criteria for respectively the modes $K^-\pi^+$, $K^-\pi^+\pi^-\pi^+$, and $K^-\pi^+\pi^0$. For $K^0_S\pi^+\pi^-$, the K^0_S candidates must satisfy the selection criteria described in Sec. III B 6.

For the decay D^0 to $K^-\pi^+\pi^0$ the combinatorial background can significantly be reduced by using the parametrization of the $K^-\pi^+\pi^0$ Dalitz distribution as provided by the Fermilab E691 experiment [31]. This distribution is dominated by the two K^* resonances ($K^{*0} \to K^-\pi^+$ or $K^{*-} \to K^-\pi^0$) and by the $\rho^+(\pi^+\pi^0)$ resonance. Therefore we select only D^0 candidates that fall in the enhanced region of the Dalitz plot as determined by the above parametrization. The π^0 must satisfy the selections described in Sec. III B 1.

The reconstructed D^0 mass resolution is about 5, 5.5, 6.5, and 11 MeV/c^2 for the decay mode $K^-\pi^+\pi^-\pi^+$, $K^0_S\pi^+\pi^-$, $K^-\pi^+$, and $K^-\pi^+\pi^0$ modes, respectively.

8. *D^{*0} selection*

The D^{*0} mesons are reconstructed in $D^0\pi^0$ and $D^0\gamma$ decay modes. The π^0 and D^0 candidates are requested to satisfy the selections described in Sec. III B 1 and III B 7 respectively. The photons from $D^{*0} \to D^0\gamma$ must fulfill the additional condition $E(\gamma) > 130$ MeV and must pass the veto against π^0 mesons as described in Sec. III B 2.

The resolution of the mass difference $\Delta m \equiv m(D^{*0}) - m(D^0)$ is about 1.3 MeV/c^2 for $D^0\pi^0$ and 7 MeV/c^2 for $D^0\gamma$.

C. Selection of B-meson candidates

The B candidates are reconstructed by combining a $D^{(*)0}$ with an h^0, with the $D^{(*)0}$ and h^0 masses constrained to their nominal value except when h^0 is an ω. One needs to discriminate between real B signal candidates and fake B candidates. The fake B candidates are originated from combinatorial backgrounds, or from other specific B modes or from the cross feed in between the similar studied color-suppressed signals.

1. *B-mesons kinematic variables*

Two kinematic variables are used in *BABAR* to select B candidates: the energy-substituted mass $m_{\rm ES}$ and the energy difference ΔE. These two variables use the constraints from the precise knowledge of the beam energies and from energy conservation in the two-body decay $\Upsilon(4S) \to B\overline{B}$. The quantity $m_{\rm ES}$ is the invariant mass of the B candidate where the B energy is set to the beam energy in the CM frame:

$$m_{\rm ES} = \sqrt{\left(\frac{s/2 + \vec{p}_0 . \vec{p}_B}{E_0}\right)^2 - |\vec{p}_B|^2}, \qquad (1)$$

and ΔE is the energy difference between the reconstructed B energy and the beam energy in the CM frame:

$$\Delta E = E^*_{D^{(*)}} + E^*_h - \sqrt{s}/2, \qquad (2)$$

where $\sqrt{s}$ is the e^+e^- center-of-mass energy. The small variations of the beam energy over the duration of the run are taken into account when calculating $m_{\rm ES}$. For the momentum $\vec{p}_i$ ($i = 0, B$) and the energy E_0, the subscripts 0 and B refer to the e^+e^- system and the reconstructed B meson, respectively. The energies $E^*_{D^{(*)}}$ and E^*_h are calculated from the measured $D^{(*)0}$ and h^0 momenta.

For the various channels of the B signal events, the $m_{\rm ES}$ distribution peaks at the B mass with a resolution of $2.6-3$ MeV/c^2, dominated by the beam energy spread, whereas ΔE peaks near zero with a resolution of $15 - 50$ MeV depending on the number of photons in the final state.

2. *Rejection of $e^+e^- \to q\overline{q}$ background*

The continuum background $e^+e^- \to q\overline{q}$, where the light quarks q are u, d, s or c quarks, creates high momentum mesons $D^{(*)0}$, π^0, $\eta^{(\prime)}$, ω that can fake the signal mesons originating from the two body decays $\overline{B}^0 \to D^{(*)0}h^0$. That background is dominated by $c\overline{c}$ processes and to a lesser extent by $s\overline{s}$ processes. Since the B mesons are produced almost at rest in the $\Upsilon(4S)$ frame, the $\Upsilon(4S) \to B\overline{B}$ event shape is spherical. By comparison, the $q\overline{q}$ events have a back-to-back jet-like shape. The $q\overline{q}$ background is therefore discriminated by employing event shape variables. The following set of variables was found to be optimal among various tested configurations:

- The thrust angle θ_T defined as the angle between the thrust axis of the B candidate and the thrust axis of the rest of event. The distribution of $|\cos(\theta_T)|$ is flat for signal and peaks at 1 for continuum background.
- Event shape monomials L_0 and L_2 defined as:

$$L_0 = \sum_i p^*_i \; ; \; L_2 = \sum_i p^*_i |\cos(\theta^*_i)|^2, \qquad (3)$$

  with p^*_i the CM momentum of the particle i that does not come from a B candidate, and θ^*_i is the angle between p^*_i and the thrust axis of the B candidate.

- The polar angle θ_B^* between the B momentum in the $\Upsilon(4S)$ frame and the beam axis. The $\Upsilon(4S)$ being vector and the B mesons being pseudoscalar, the angular distribution is proportional to $\sin^2(\theta_B^*)$ for signal and roughly flat for background.

These four discriminating variables are combined in a Fisher discriminant built with the `TMVA` [32] toolkit package. An alternate approach employing a multi-layers perception artificial neural network with two hidden layer within the same framework was tested and showed marginal relative gain, therefore the Fisher discriminant is used.

The Fisher discriminant $\mathcal{F}_{shape}$ is trained with signal MC events and off-peak data events. In order to maximize the number of off-peak events all the $\overline{B}^0 \to D^{(*)0}h^0$ modes are combined. We retain signal MC events with $m_{\rm ES}$ in the signal region $5.27-5.29$ MeV/c^2 and off-peak data events with $m_{\rm ES}$ in the range $5.25-5.27$ MeV/c^2, accounting for half of the 40 MeV CM energy shift below the $\Upsilon(4S)$ resonance. The training and testing of the multivariate classifier are performed with the non-overlapping data samples of equal size obtained from a cocktail of 20000 MC simulation signal events and from 20000 off-peak events. The obtained Fisher formula is:

$$\mathcal{F}_{shape} = 2.36 - 1.18 \times |\cos(\theta_T)| + 0.20 \times L_0 - 1.01 \times L_2 - 0.80 \times |\cos(\theta_B^*)|. \quad (4)$$

The $q\overline{q}$ background is reduced by applying a selection cut on $\mathcal{F}_{shape}$. The selection is optimized for each of the 72 possible $\overline{B}^0$ signal modes by maximizing the statistical significance with signal MC against generic MC $e^+e^- \to q\overline{q}$, $q \neq b$. This requirement for the various decay modes retains between about 30% and 97% of B signal events, while rejecting between about 98% and 35% of the light $q\overline{q}$ pairs background.

3. Rejection of other specific backgrounds

The ω mesons in $\overline{B}^0 \to D^0\omega$ decays are longitudinally polarized. We define the *normal angle* θ_N [10, 33] as the the angle between the normal to the plane of the three daughter pions in the ω frame and the line-of-flight of the $\overline{B}^0$ meson in the ω rest frame. That definition is the equivalent of the two-body helicity angle for the three-body decay. To describe the three-body decay distribution of $\omega \to \pi^+\pi^-\pi^0$, we define the *Dalitz angle* θ_D [10] as the angle between the π^0 momentum in the ω frame and the π^+ momentum in the frame of the pair of charged pions.

The signal distribution is proportional to $\cos^2(\theta_N)$ and $\sin^2(\theta_D)$, while the combinatorial background distribution is roughly flat as a function of $\cos(\theta_N)$ and $\cos(\theta_D)$. These two angles are combined in a Fisher discriminant $\mathcal{F}_{hel}$ built from signal MC events and generic $q\overline{q}$ and $B\overline{B}$ MC events:

$$\mathcal{F}_{hel} = -1.41 - 1.01 \times |\cos(\theta_D)| + 3.03 \times |\cos(\theta_N)|. \quad (5)$$

We require $\overline{B}^0 \to D^0\omega$ candidates to satisfy $\mathcal{F}_{hel} > -0.1$, to obtain an efficiency (rejection) on signal (background) of about 85% (62%).

We also exploit the angular distribution properties in the decay $D^{*0} \to D^0\pi^0$ to reject combinatorial background. We define the helicity angle θ_{D^*} as the angle between the line-of-flight of the D^0 and that of the D^{*0}, both evaluated in the D^{*0} rest frame. The angular distribution is proportional to $\cos^2(\theta_{D^*})$ for signal and roughly flat for combinatorial background. Although in principle such a behavior could be employed for $\overline{B}^0 \to D^{*0}\pi^0$, $D^{*0}\eta$, and $D^*\eta'$, a selection on $|\cos(\theta_{D^*})|$ significantly improves the statistical significance for the $\overline{B}^0 \to D^{*0}\pi^0$ mode only. Therefore D^{*0} candidates coming from the decay $\overline{B}^0 \to D^{*0}\pi^0$ are required to satisfy $|\cos(\theta_{D^*})| > 0.4$ with an efficiency (rejection) on signal (background) of about 91% (33%).

A major $B\overline{B}$ background contribution in the analysis of the $\overline{B}^0 \to D^{(*)0}\pi^0$ channel comes from the color-allowed decay $B^- \to D^{(*)0}\rho^-$. If the charged pion (mostly slow) from the decay $\rho^- \to \pi^-\pi^0$ is omitted in the reconstruction of the $\overline{B}^0$ candidate, $B^- \to D^{(*)0}\rho^-$ events can mimic the $D^{(*)0}\pi^0$ signal. Moreover, the $\mathcal{B}(B^- \to D^{(*)0}\rho^-)$ are $30-50$ times larger than that of the $\overline{B}^0 \to D^{(*)0}\pi^0$ modes, and not precisely known ($\delta\mathcal{B}/\mathcal{B} = 13.4\% - 17.3\%$ [25]). A veto is applied to reduce this background. For each $\overline{B}^0 \to D^{(*)0}\pi^0$ candidate, we combine any remaining negatively charged track in the event to reconstruct a B^- candidate in the decay mode $D^{(*)0}\rho^-$. If the reconstructed B^- candidate satisfies $m_{\rm ES}(B^-) > 5.27$ GeV/c^2, $|\Delta E(B^-)| < 100$ MeV, and $|m(\rho^-) - m(\rho^-)_{\rm PDG}| < 250$ MeV/c^2, then the initial $\overline{B}^0$ candidate is rejected. For the analysis of the decay mode $\overline{B}^0 \to D^0\pi^0$ ($B^- \to D^{*0}\pi^0$), the veto retains about 90% (82%) of signal and rejects about 67% (56%) of $B^- \to D^0\rho^-$ and 44% (66%) of $B^- \to D^{*0}\rho^-$ background.

4. Choice of the "best" B candidate in the event

The average number of $\overline{B}^0 \to D^{(*)0}h^0$ candidate per event after all selections ranges between 1 and 1.6 depending on the complexity of the sub-decays. We keep one B candidate per mode per event. The chosen B is the one with the smallest value of

$$\chi^2_B = \left(\frac{m(D^0) - m(D^0)_{\rm mean}}{\sigma_{m(D^0)}}\right)^2 + \left(\frac{m(h^0) - m(h^0)_{\rm mean}}{\sigma_{m(h^0)}}\right)^2, \quad (6)$$

for D^0h^0 modes and of

$$\chi_B^2 = \left(\frac{m(D^0) - m(D^0)_{\rm mean}}{\sigma_{m(D^0)}}\right)^2 + \left(\frac{m(h^0) - m(h^0)_{\rm mean}}{\sigma_{m(h^0)}}\right)^2 + \left(\frac{\Delta m - \Delta m_{\rm mean}}{\sigma_{\Delta m}}\right)^2, \quad (7)$$

for the $D^{*0}h^0$ modes. The quantities $\sigma_{m_{D^0}}$ and $\sigma_{m_{h^0}}$ ($m(D^0)_{\rm mean}$ and $m(h^0)_{\rm mean}$) are the resolution (mean) of the mass distributions. The quantities $\Delta m_{\rm mean}$ and $\sigma_{\Delta m}$ are respectively the mean and resolution of the Δm ($\equiv m(D^{*0}) - m(D^0)$) distributions. These quantities are obtained from fits of the mass distribution of true simulated candidates selected from signal MC simulations.

The probability of choosing the true $\overline{B}^0$ candidate in the event according to the above criteria ranges from 71 to 100%. The cases with lower probabilities correspond to the $D^{(*)0}h^0$ modes with high neutral multiplicity.

5. *Selection efficiencies*

The branching fraction of the $\overline{B}^0 \to D^{(*)0}h^0$ decays is computed as:

$$\mathcal{B}(\overline{B}^0 \to D^{(*)0}h^0) = \frac{N_S}{N_{B\bar{B}} \cdot \mathcal{E} \cdot \mathcal{B}_{sec}}, \quad (8)$$

where $\mathcal{B}_{sec}$ is the product of the branching fractions associated with the secondary decays of the $D^{(*)0}$ and h^0 mesons for the each of the 72 decay channel considered in this paper [25]. $N_{B\bar{B}}$ is the number of $B\overline{B}$ pairs in data and N_S is the number of signal events remaining after all the selections. The quantity $\mathcal{E}$ is the total signal efficiency including reconstruction (detector and trigger acceptance) and analysis selections. It is computed from each of the 72 exclusive high statistics MC simulation samples.

The selection efficiency from MC simulation is slightly different from the efficiency in data. The MC efficiency and its systematic uncertainty therefore has to be adjusted according to control samples. For the reconstruction of π^0/γ, the efficiency corrections are obtained from detailed studies performed with a high statistics and high purity control sample of π^0 mesons produced in $\tau \to \rho(\pi\pi^0)\nu_\tau$ decays normalized to $\tau \to \pi\nu_\tau$, to unfold tracking effects. Such corrections are validated against studies performed on the relative ratio of the number of detected D^0 mesons in the decays $D^0 \to K^-\pi^+\pi^0$ and $D^0 \to K^-\pi^+$, and produced in the decay of D^{*+} mesons from $e^+e^- \to c\bar{c}$ events. The relative data/simulation efficiency measurements for charged tracks are similarly based on studies of track mis-reconstruction using $e^+e^- \to \tau^+\tau^-$ events. On one side the events are tagged from a lepton in the decay $\tau^- \to l^-\bar{\nu}_l\nu_\tau$ and on the other side one reconstructs the 2 or 3 tracks from the decay $\tau^+ \to \pi^+\pi^-h^+\bar{\nu}_\tau$ (the $\pi^+\pi^-$ can be originated from a ρ^0 resonance). The simulated efficiency of charged particle identification is compared to the efficiency computed in data with control samples of kaons selected with detector independent considerations from $D^{*+} \to D^0(K^-\pi^+)\pi^+$ produced in $e^+e^- \to c\bar{c}$ events. The simulation efficiency on K_S^0 candidates is modified using a data sample of K_S^0, mainly arising from the continuum processes e^+e^- into $q\bar{q}$.

The efficiency corrections for the selection criteria applied to $D^{(*)0}$ candidates and on the Fisher discriminant ($\mathcal{F}_{hel}$) for the continuum $q\bar{q}$ rejection are obtained from studies of a $B^- \to D^{(*)0}\pi^-$ control sample. This abundant control sample is chosen for its kinematic similarity with $\overline{B}^0 \to D^{(*)0}h^0$. The corrections are computed from the ratios $\mathcal{E}_{\rm rel.}({\rm data})/\mathcal{E}_{\rm rel.}({\rm MC})$, where the relative efficiencies $\mathcal{E}_{\rm rel.}$ are computed with the signal yields as obtained from fits to $m_{\rm ES}$ distributions of $B^- \to D^{(*)0}\pi^-$ candidates in data and MC simulation, before and after applying the various selections. The obtained results are checked with the color-allowed control sample $B^- \to D^{(*)0}\rho^-$, which has slightly different kinematics due to the relatively higher mass of the ρ^-, and therefore validates those corrections for the modes such as $D^{(*)0}\eta'$.

The reconstruction efficiency of $\overline{B}^0 \to D^{*0}\omega$ depends on the angular distribution, which is not yet known. To evaluate this efficiency we combine a set of properly weighted fully longitudinally and fully transversely polarized MC samples, according to the fraction of longitudinal polarization ($f_L = 66.5$ %) that we measure in this paper (see Sec. VI).

D. Fit procedure and data distributions

We present the fits used to extract the branching fractions $\mathcal{B}$. For each of the 72 possible $\overline{B}^0 \to D^{(*)0}h^0$ subdecay modes, using an iterative procedure, we fit the ΔE distribution in the range $-280 < \Delta E < 280$ MeV for $m_{\rm ES} > 5.27$ GeV/c^2 to get the signal (N_S) and background yields. The use of the ΔE distribution allows us to model and adjust the complex non-combinatoric B background structure without relying completely on simulation.

The data samples corresponding to each $\overline{B}^0$ decay mode are disjoint and the fits are performed independently for each mode. According to their physical origin, four categories of events with differently shaped ΔE distributions are separately considered: signal events, cross-feed events, peaking background events, and combinatorial background events. The event (signal and background) yields are obtained from unbinned extended maximum likelihood (ML) fits. We write the extended likelihood $\mathcal{L}$ as

$$\mathcal{L} = \frac{e^{-n}}{N!} n^N \prod_{j=1}^{N} f(\Delta E_j|\theta, n), \quad (9)$$

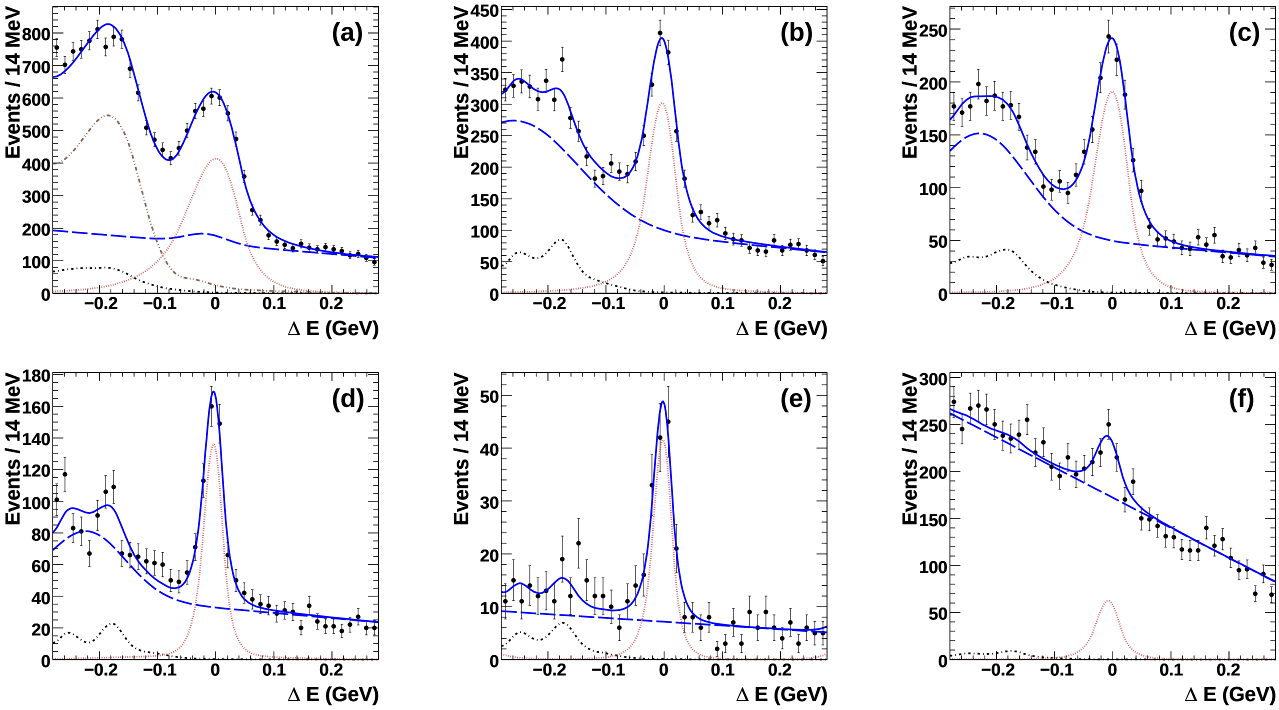

FIG. 2. Fit of ΔE distributions in data for modes $\overline{B}^0 \to D^0\pi^0$ (a), $\overline{B}^0 \to D^0\omega$ (b), $\overline{B}^0 \to D^0\eta(\gamma\gamma)$ (c), $\overline{B}^0 \to D^0\eta(\pi\pi\pi^0)$ (d), $\overline{B}^0 \to D^0\eta'(\pi\pi\eta)$ (e), and $\overline{B}^0 \to D^0\eta'(\rho^0\gamma)$ (f). The dots with error bars are data, the blue solid curve is the fitted total PDF, the red dotted curve is the signal PDF, the black dotted-dashed curve is the cross-feed PDF, the brown double dotted-dashed curve is the $B^- \to D^{(*)0}\rho^-$ PDF, and the long blue dashed curve is the combinatorial background PDF.

where θ indicates the set of parameters which are fitted from the data. N is the total number of signal and background events, and $n = \sum_i N_i$ is the expectation value for the total number of events. The sum runs over the different signal and background categories i, which PDF and characteristics will be detailed below. The total probability density function (PDF) $f(\Delta E_j|\theta, n)$ is written as the sum over the different signal and background categories

$$f(\Delta E_j|\theta, n) = \frac{\sum_i N_i f_i(\Delta E_j|\theta)}{n}, \tag{10}$$

where $f_i(\Delta E|\theta)$ is the PDF of the various i categories: signal or background components. Some of the PDF component parameters are fixed from the MC simulation (see details in the following sections).

The individual corresponding branching ratios are computed and then combined as explained in Sec. V.

1. *Signal contribution*

All of the 72 possible reconstructed $\overline{B}^0$ channels contain at least one photon. Due to the possible energy losses of early showering γ's in the detector material before the EMC, the ΔE shape for signal is modeled by the so-called *modified Novosibirsk* PDF [30]. A Gaussian PDF is added to the modes with a large ΔE resolution to describe mis-reconstructed events. The signal shape parameters are estimated from a ML fit to the distributions of simulated signal events in the high statistics exclusive decay modes.

2. *Cross-feed contribution*

We call "cross feed" the events from all of the $D^{(*)0}h^0$ modes, except the one we reconstruct, that pass the complete selection and that are reconstructed in the given mode. The cross-feed events are a non-negligible part of the ΔE peak in some of the modes, and the signal event yield must be corrected for these cross-feed events. As the various channels are studied in parallel, we use an iterative procedure to account for those contributions in the synchronous measurements (see Sec. III D 5).

The dominant cross-feed contribution to $\overline{B}^0 \to D^0h^0$ comes from the companion channel $\overline{B}^0 \to D^{*0}h^0$, when the π^0/γ from the D^{*0} decay is not reconstructed. Such cross-feed events are shifted in ΔE by by approximately the mass of π^0 (-135 MeV), with a long tail from $D^{*0}(\to D^0\gamma)h^0$ leaking into the signal region. Similarly, the channel $\overline{B}^0 \to D^{*0}h^0$ receives a cross-feed contribution from the associated decay mode $\overline{B}^0 \to D^0h^0$ and there is a cross-contamination in between the $D^{*0} \to D^0\pi^0$ and

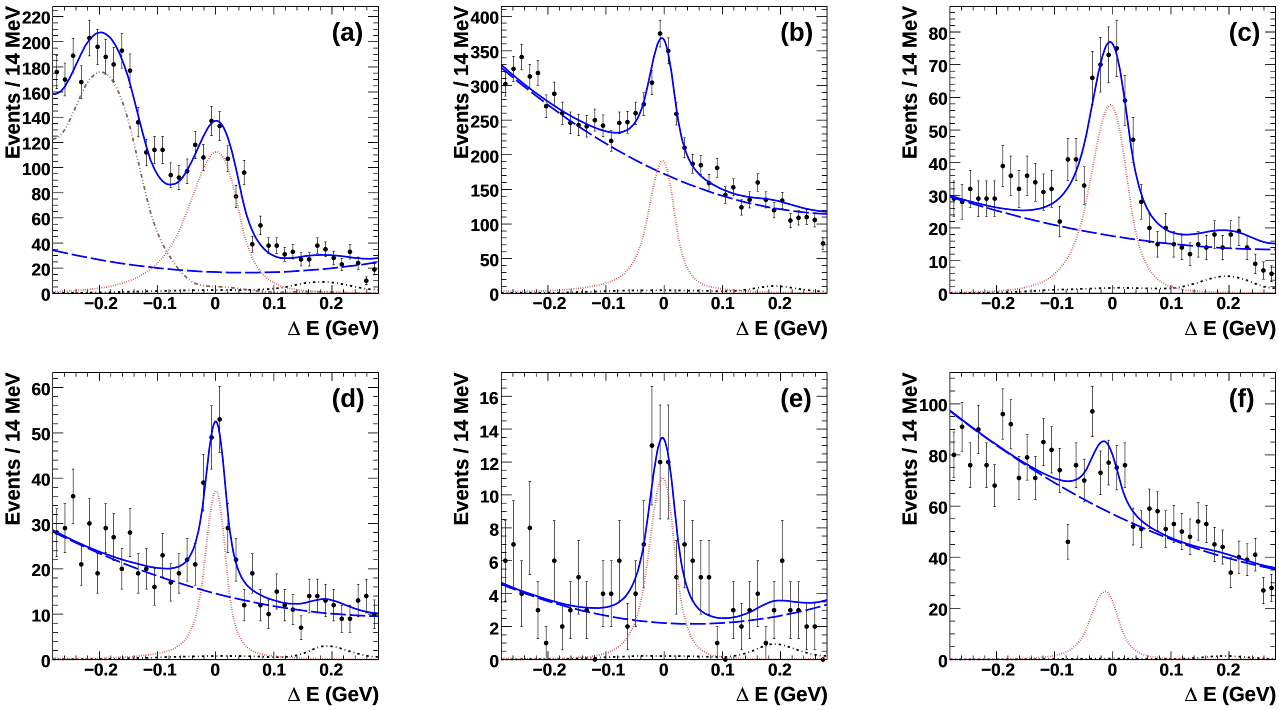

FIG. 3. Fit of ΔE distributions in data for modes $\overline{B}^0 \to D^{*0}\pi^0$ (a), $\overline{B}^0 \to D^{*0}\omega$ (b), $\overline{B}^0 \to D^{*0}\eta(\gamma\gamma)$ (c), $\overline{B}^0 \to D^{*0}\eta(\pi\pi\pi^0)$ (d), $\overline{B}^0 \to D^{*0}\eta'(\pi\pi\eta)$ (e), and $\overline{B}^0 \to D^{*0}\eta'(\rho^0\gamma)$ (f) where the D^{*0} mesons decay into the signal mode $D^0\pi^0$. A detailed legend is provided in the caption of Fig. 2.

$D^{*0} \to D^0\gamma$ channels.

The main cross-feed contributions from the other reconstructed $\overline{B}^0$ color-suppressed modes are listed in Table I. For each signal mode, different cross feeds are summed and their contribution is estimated with a histogram-based PDF built from the various signal MC samples.

TABLE I. Main cross feeds between signal modes and for a given D^0 decay mode. For a given $D^{*0}h^0$ mode the cross feed coming from the sub-decay $D^{*0} \to D^0\pi^0$ into $D^{*0} \to D^0\gamma$ is relatively larger than in the mirror case.

B mode	Cross-feed modes
D^0h^0	$D^{*0}h^0$
$D^{*0}(D^0\pi^0)h^0$	$D^{*0}(D^0\gamma)h^0$, D^0h^0
$D^{*0}(D^0\gamma)h^0$	$D^{*0}(D^0\pi^0)h^0$, D^0h^0

3. *Peaking $B\overline{B}$ background contributions*

The major background in the reconstruction of $\overline{B}^0 \to D^{(*)0}\pi^0$ comes from the decays $B^- \to D^{(*)0}\rho^-$ (see Sec. III C 3). Their contribution is modeled by a separate histogram-based PDF built from the high statistics exclusive signal MC simulation samples. The individual distributions of the two backgrounds $B^- \to D^0\rho^-$ and $B^- \to D^{*0}\rho^-$ that pass the $\overline{B}^0 \to D^{(*)0}\pi^0$ selections, including the specific veto requirement as described in Sec. III C 3, cannot be distinguished. As a consequence, given the large uncertainty on their branching fractions, the overall normalization of $B^- \to D^{(*)0}\rho^-$ PDF is left floating but the relative ratio $N(B^- \to D^{*0}\rho^-)/N(B^- \to D^0\rho^-)$ of the PDF normalization is fixed. The value of this ratio is extracted directly from the data by reconstructing exclusively each of the $B^- \to D^{(*)0}\rho^-$ modes rejected by the veto requirements. Those fully reconstructed B^--mesons differ from the $B^- \to D^{(*)0}\rho^-$, that pass all the $\overline{B}^0 \to D^{(*)0}\pi^0$ selections, by the additional selected soft charged π originated from the ρ^- meson. The relative correction on that ratio for events surviving the veto selection is then computed using the MC simulation for truly generated $B^- \to D^{(*)0}\rho^-$ decays. A systematic uncertainty on that assumption is assigned (see Sec. IV).

In the cases of $\overline{B}^0 \to D^{(*)0}\omega/\eta(\to \pi^+\pi^-\pi^0)$ modes, additional contributions come from the B decay modes $D^{(*)}n\pi\pi^{(0)}$, where $n = 1,\ 2,$ or 3, and through intermediate resonances such as ω and $\rho'^-(\to \omega\pi^-)$. These peaking backgrounds are modeled by a first-order polynomial PDF plus a Gaussian PDF determined from the generic $B\overline{B}$ MC simulation. The relative normalization of that Gaussian PDF component is left floating in the

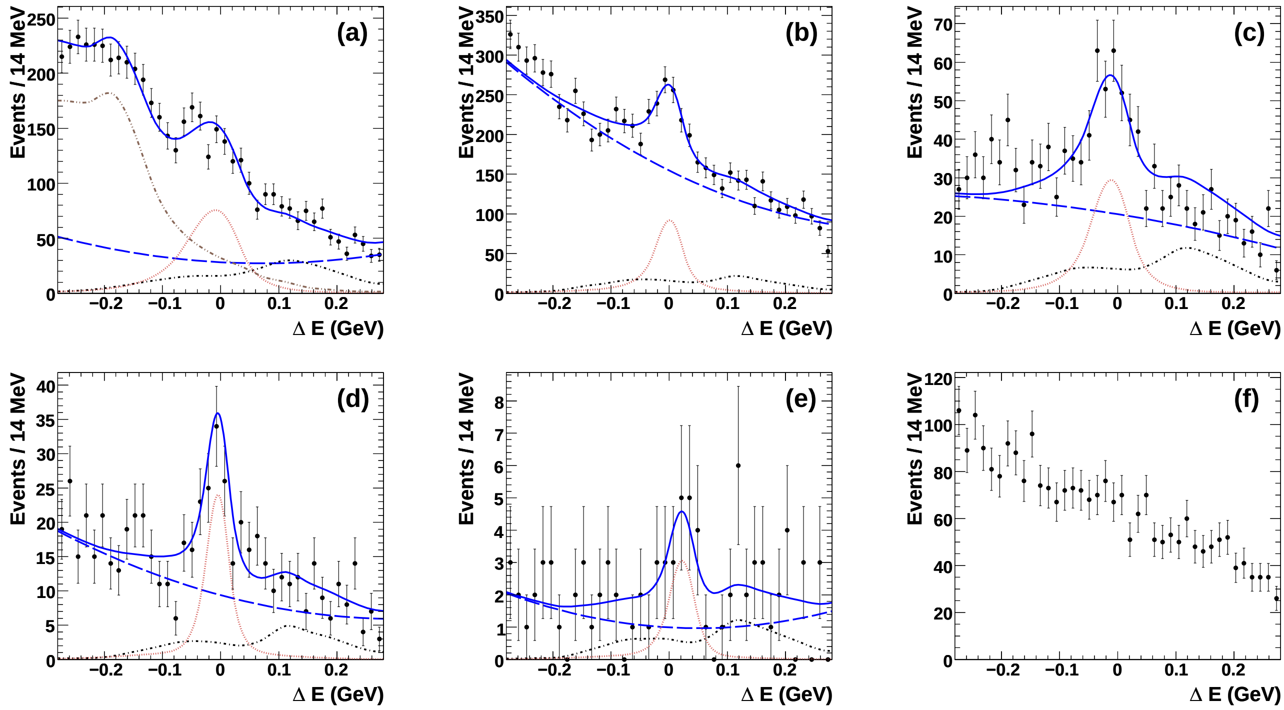

FIG. 4. Fit of ΔE distributions in data for modes $\overline{B}^0 \to D^{*0}\pi^0$ (a), $\overline{B}^0 \to D^{*0}\omega$ (b), $\overline{B}^0 \to D^{*0}\eta(\gamma\gamma)$ (c), $\overline{B}^0 \to D^{*0}\eta(\pi\pi\pi^0)$ (d), and $\overline{B}^0 \to D^{*0}\eta'(\pi\pi\eta)$ (e), where the D^{*0} mesons decay into the signal mode $D^0\gamma$. The unfitted ΔE distribution of $\overline{B}^0 \to D^{*0}(D^0\gamma)\eta'(\rho^0\gamma)$ candidates is also displayed (f). A detailed legend is provided in the caption of Fig. 2.

fit, since the $\mathcal{B}$ of the B decay modes $D^{(*)}n\pi\pi^{(0)}$ are not necessarily precisely known [25].

4. *Combinatorial background contribution*

The shape parameters of the combinatorial background PDFs are obtained from ML fits to the generic $B\overline{B}$ and continuum MC, where all signal, cross feeds and above-discussed peaking $B\overline{B}$ background events have been removed. The combinatorial background from $B\overline{B}$ and $q\overline{q}$ are summed and modeled by a second-order polynomial PDF.

5. *Iterative fitting procedure*

We fit the ΔE distribution using the PDFs for the signal, for the cross feed, for the peaking background, and for the combinatorial background as detailed in the previous sections. The normalization for the signal, for the peaking $B\overline{B}$ backgrounds, and for the combinatorial background components are allowed to float in the fit. The mean of the signal PDF is left floating for the sum of $D^{(*)0}$ sub-decays. For each D^0 sub-mode, the signal mean PDF is fixed to the value obtained from the fit to the sum of D^0 sub-modes. Those free parameters are extracted by maximizing the unbinned extended likelihood to the ΔE distribution defined in Eqs. 9 and 10. Other PDF parameters are fixed from fit results obtained with MC simulations, when studying separately each of the signal and background categories.

In the global event yield extraction of all the various $\overline{B}^0 \to D^{(*)0}h^0$ color-suppressed signals studied in this paper, a given mode can be signal and cross feed to other modes at the same time. In order to use the $\mathcal{B}$ computed in this analysis, the yield extraction is performed through an iterative fit successively on $D^{*0}h^0$ and D^0h^0. The normalization of cross-feed contribution from $D^{(*)0}h^0$ is then fixed to the $\mathcal{B}$ measured in the previous fit iteration. For the cross-feed contributions, the PDG branching fraction [25] values are used as starting points. This iterative method converges quickly to a stable value of $\mathcal{B}$'s, with variation less than 10% of statistical uncertainty, in less than 5 iterations.

We check the absence of bias in our fit procedure by studying pseudo-experiments with a large number of different samples for the various signals. The extraction procedure is applied to these samples where background events are generated and added from the fitted PDFs. The signal samples are assembled from non-overlapping samples corresponding to the exclusive high statistics MC signals, with yields corresponding to the MC-generated value of the branching fraction $\mathcal{B}_{gen}$. No significant biases are found.

6. Data distributions and event yields from summed sub-decay modes

The fitting procedure is applied to data at the very last stage of the blind analysis. Though the event yields and $\mathcal{B}$ measurements are performed separately for each of the 72 considered sub-decay modes, we illustrate here, in a compact manner, the magnitude of the signal and background component yields and of the statistical significances of the various channels $\overline{B}^0 \to D^{(*)0}h^0$. To do that, we sum together the D^0 sub-modes. The fitted ΔE distributions, for the sum of D^0 sub-modes, are given in Figs. 2, 3, and 4, for respectively the $\overline{B}^0 \to D^0h^0$, $D^{*0}(\to D^0\pi^0)h^0$, and $D^{*0}(\to D^0\gamma)h^0$ modes.

The signal and background yields obtained from the fit to the summed sub-mode data for the $\overline{B}^0 \to D^{(*)0}h^0$ are presented in Table II, with the corresponding statistical significance. The statistical significance is calculated in the signal region $|\Delta E| < 2.5\sigma$, from the cumulative Poisson probability p to have a background statistical fluctuation reaching the observed data yield:

$$p = \sum_{k=N_{cand}}^{+\infty} \frac{e^{-\nu}}{k!}\nu^k, \qquad (11)$$

where N_{cand} is the total number of selected candidates in the signal region and ν the mean value of the total expected background, as extracted from the fit. This probability is then converted into a number of equivalent one-sided standard deviations:

$$N_\sigma = \sqrt{2}\ \texttt{erfcInverse}(p/2), \qquad (12)$$

The function `erfcInverse` is the inverse of the complementary error function of `erf` (see statistics section in [25]).

The signal and background yields are computed from the fit parameters and integrated in a ΔE window of $\pm 2.5\sigma$ (where σ is the signal resolution).

The majority of channels present a clear and significant signal. In particular, the modes $D^0\eta'(\pi\pi\eta(\gamma\gamma))$ and $D^0\eta'(\rho^0\gamma)$ are observed for the first time.

Before performing the final unblinded fits on data, among the various 72 initial possible decay channels, several sub-decay modes have been discarded. The decisions to remove those sub-modes has been taken according to analyses performed on MC simulation, as no significant signals are expected and confirmed in data (see for example Fig. 4 (bottom right)). The discussed channels are: $\overline{B}^0 \to D^{(*)0}\eta'$ and $D^{*0}(D^0\gamma)\eta(\pi\pi\pi^0)$, where $D^0 \to K^0_S\pi^+\pi^-$, $D^{*0}(D^0\gamma)\eta'(\pi\pi\eta)$, where $D^0 \to K^-\pi^+\pi^-\pi^+$, as well as the whole channel $D^{*0}(D^0\gamma)\eta'(\rho^0\gamma)$. Those are sub-modes with poor signal efficiency, caused by large track multiplicity or modest D^0 secondary $\mathcal{B}$'s, such that the expected signal yields are very low. In addition, much larger background contributions are expected. We concluded that adding such channels in the global combinations would degrade the $\mathcal{B}$ measurements.

IV. SYSTEMATIC UNCERTAINTIES ON BRANCHING FRACTIONS

There are several possible sources of systematic uncertainties in this analysis, whose combinations are summarized in Table III.

The categories "π^0/γ detection" and "Tracking" account respectively for the systematics on the reconstruction of π^0/γ and for charged particle tracks, and are taken as the uncertainty on the efficiency correction computed in the studies of τ decays from $e^+e^- \to \tau^+\tau^-$ events (see Sec. III C 5).

Similarly, the systematic uncertainties on kaon identification and on the reconstruction of K^0_S mesons are estimated from the uncertainties on MC efficiency corrections computed in the study of pure samples of kaons and K^0_S mesons compared to data (see Sec. III C 5).

The uncertainty on the secondary $\mathcal{B}$ is a combination of the uncertainties on each $\mathcal{B}$ of the $D^{(*)0}$ and h^0 sub-mode (including secondary decays into detected stable particles). Correlations between the different channels were accounted for [25].

The uncertainty related to the number of $B\overline{B}$ pairs and the binomial uncertainty related to the limited available MC samples statistics when computing the efficiency of various selection criteria are also included.

The systematics on the resonance mass selections are computed as the relative difference of signal yield when the values of the mass means and mass resolutions are taken from a fit to the data. The uncertainties for the $q\bar{q}$ rejection and the $D^{(*)0}$ selections are obtained from the study performed on the control sample $B^- \to D^{(*)0}\pi^-$ and are estimated as the uncertainty on the efficiency correction ratio: $\mathcal{E}_{\rm rel.}(\text{data})/\mathcal{E}_{\rm rel.}(\text{MC})$, including the correlations between the samples before and after selections (see Sec. III C 5). The uncertainties for the cuts on ρ^0 and $D^0\omega$ helicities are obtained by varying the selection cut values by $\pm 10\%$ around the maximum of statistical significance. All uncertainties on resonances selections are combined in the category "Resonances selection".

The uncertainty quoted for "ΔE Fit" gathers the uncertainties on the shapes of signal and background PDF, and on the cross-feed $\mathcal{B}$. For the modes $D^{(*)0}\pi^0/\eta(\gamma\gamma)$, with high momentum γ in the final state, the shape difference between data and MC simulation on energy scale and resolution for neutrals is estimated from a study of the high statistics control sample $B^- \to D^0(K^-\pi^+)\rho^-(\pi^0\pi^-)$, which yields the difference between data and MC simulation: $|\Delta E_{\rm mean}| \simeq 5.7$ MeV, for the mean and $|\Delta E_{\rm resolution}| \simeq 3.3$ MeV, for the resolution. For those modes, the uncertainty on signal shape is obtained by varying the signal PDF mean by ± 5.7 MeV and the width by ± 3.3 MeV. For the other $\overline{B}^0$ signal modes, each PDF parameter is varied within the $\pm 1\sigma$ MC simulation uncertainty , and the relative difference on fitted event yield is taken as a systematic uncertainty. The various parameters are varied one at a time. The relative differences while varying the ΔE PDF parameters

TABLE II. Number of signal events (N_S), cross feed ($N_{\rm cf}$), and combinatorial background ($N_{\rm combi}$) and $B^- \to D^{(*)0}\rho^-$ ($N_{\rm D\rho}$) computed from the ΔE fit to data, as well as the statistical significance in number of standard deviations (see text). The quoted uncertainties are statistical only.

$\overline{B}^0 \to$ (decay channel)	N_S	$N_{\rm combi}$	$N_{\rm cf}$	$N_{\rm D\rho}$	Statistical significance
$D^0\pi^0$	3429 ± 123	2625 ± 75	97 ± 3	700 ± 14	41
$D^0\eta(\gamma\gamma)$	1022 ± 55	532 ± 14	13 ± 1	-	36
$D^0\eta(\pi\pi\pi^0)$	411 ± 29	191 ± 6	2 ± 0	-	23
$D^0\omega$	1374 ± 120	886 ± 25	18 ± 2	-	38
$D^0\eta'(\pi\pi\eta(\gamma\gamma))$	122 ± 13	41 ± 3	-	-	14
$D^0\eta'(\rho^0\gamma)$	234 ± 40	1253 ± 17	1 ± 0	-	7.4
$D^{*0}(D^0\pi^0)\pi^0$	883 ± 40	268 ± 21	39 ± 2	175 ± 5	34
$D^{*0}(D^0\gamma)\pi^0$	622 ± 47	469 ± 33	295 ± 23	602 ± 20	17
$D^{*0}(D^0\pi^0)\eta(\gamma\gamma)$	338 ± 25	201 ± 9	17 ± 1	-	19
$D^{*0}(D^0\gamma)\eta(\gamma\gamma)$	187 ± 24	254 ± 12	85 ± 11	-	8.7
$D^{*0}(D^0\pi^0)\eta(\pi\pi\pi^0)$	123 ± 15	90 ± 4	5 ± 1	-	11
$D^{*0}(D^0\gamma)\eta(\pi\pi\pi^0)$	88 ± 14	65 ± 4	16 ± 3	-	7.6
$D^{*0}(D^0\pi^0)\omega$	806 ± 48	1365 ± 18	33 ± 2	-	20
$D^{*0}(D^0\gamma)\omega$	414 ± 44	1290 ± 19	132 ± 14	-	10
$D^{*0}(D^0\pi^0)\eta'(\pi\pi\eta)$	45 ± 8	18 ± 2	2 ± 0	-	8.5
$D^{*0}(D^0\gamma)\eta'(\pi\pi\eta)$	12 ± 5	8 ± 1	5 ± 2	-	3.2
$D^{*0}(D^0\pi^0)\eta'(\rho^0\gamma)$	115 ± 25	487 ± 11	3 ± 1	-	5.4

TABLE III. Combined contributions to the $\mathcal{B}(\overline{B}^0 \to D^{(*)0}h^0)$ relative systematic uncertainties (%).

Sources	$\Delta\mathcal{B}/\mathcal{B}$(%) for the $\overline{B}^0$ decay									
	$D^0\pi^0$	$D^0\eta(\gamma\gamma)$	$D^0\eta(\pi\pi\pi^0)$	$D^0\omega$	$D^0\eta'(\pi\pi\eta)$	$D^0\eta'(\rho^0\gamma)$	$D^{*0}\pi^0$	$D^{*0}\eta$	$D^{*0}\omega$	$D^{*0}\eta'$
π^0/γ detection	3.5	3.5	3.6	3.6	3.7	2.3	6.2	5.5	5.7	5.8
Tracking	0.9	0.9	1.6	1.7	1.6	1.6	0.9	1.1	1.6	1.6
Kaon ID	1.0	1.1	1.1	1.1	1.2	1.1	1.1	1.1	1.1	1.2
K^0_S reconstruction	0.7	0.7	0.6	0.8	0.6	0.6	0.4	0.3	0.5	-
Secondary $\mathcal{B}$	1.6	1.6	2.0	1.8	2.3	2.4	5.1	5.7	5.5	5.1
$B\overline{B}$ counting	1.1	1.1	1.1	1.1	1.1	1.1	1.1	1.1	1.1	1.1
MC statistics	0.1	0.2	0.3	0.2	0.4	0.4	0.2	0.2	0.3	0.3
Resonances selection	0.3	0.4	0.2	1.0	0.3	1.0	0.2	0.1	0.1	1.2
ΔE fit	2.1	2.2	1.3	2.1	1.1	2.1	1.0	0.6	1.4	0.5
Continuum $q\bar{q}$ rejection	0.1	0.1	0.1	0.1	0.1	0.1	0.1	0.1	0.1	0.1
$D^{(*)0}\rho^-$ background	1.8	-	-	-	-	-	5.6	-	-	-
$D^{*0}\omega$ polarization	-	-	-	-	-	-	-	-	1.4	-
Total	5.1	4.9	4.9	5.3	5.1	4.7	9.6	8.2	8.5	8.2

are then summed up in quadrature. This sum is taken as a systematic uncertainty on ΔE.

The uncertainty on the continuum background shape is estimated from the difference of the PDF fitted on generic MC simulation with that of the PDF fitted in the $m_{\rm ES}$ sideband $5.24 < m_{\rm ES} < 5.26$ GeV/c^2 in data. When a Gaussian is added to the combinatorial background shape, to model additional peaking $B\overline{B}$ background contributions (see Sec. III D 3), the related uncertainty is computed by varying its means and resolution by $\pm 1\sigma$.

We account for possible differences in the PDF shape of the $B^- \to D^{(*)0}\rho^-$ background that is modeled by a non-parametric PDF. As above it is obtained by shifting and smearing the PDF mean and resolution by ± 5.7 MeV and ± 3.3 MeV respectively. The non-parametric PDF is therefore convoluted with a Gaussian with the previously defined mean and width values. The quadratic sum of the various changes on the signal event yield is taken as a systematic uncertainty.

The relative ratio of the $B^- \to D^{*0}\rho^-$ and $B^- \to D^0\rho^-$ backgrounds for the studies of the modes $\overline{B}^0 \to D^{(*)0}\pi^0$ has been fixed to the data for rejected B^- events with the veto described in Sec. III C 3. The effect of such a veto on that ratio is then computed from MC simulation. We assign as a conservative systematic uncertainty half of the difference between the nominal result and

TABLE IV. Branching fractions of channels $\overline{B}^0 \to D^{(*)0}h^0$ measured in the different secondary decay modes. The first uncertainty is statistical and the second is systematic. The cells with "-" correspond to channels that have been discarded after the analysis on simulation, and confirmed with data, as no significant signal is expected or seen for them.

$\mathcal{B}(\overline{B}^0 \to)$ ($\times 10^{-4}$)	$D^0 \to K\pi$	$D^0 \to K3\pi$	$D^0 \to K\pi\pi^0$	$D^0 \to K^0_S\pi^+\pi^-$
$D^0\pi^0$	$2.49 \pm 0.13 \pm 0.16$	$2.69 \pm 0.15 \pm 0.17$	$2.97 \pm 0.15 \pm 0.25$	$2.90 \pm 0.28 \pm 0.23$
$D^0\eta(\gamma\gamma)$	$2.46 \pm 0.18 \pm 0.14$	$2.56 \pm 0.19 \pm 0.16$	$2.37 \pm 0.20 \pm 0.20$	$2.62 \pm 0.37 \pm 0.21$
$D^0\eta(\pi\pi\pi^0)$	$2.59 \pm 0.27 \pm 0.12$	$2.65 \pm 0.30 \pm 0.14$	$2.48 \pm 0.29 \pm 0.20$	$2.28 \pm 0.54 \pm 0.18$
$D^0\omega$	$2.59 \pm 0.18 \pm 0.20$	$2.34 \pm 0.19 \pm 0.15$	$2.42 \pm 0.20 \pm 0.21$	$3.17 \pm 0.39 \pm 0.24$
$D^0\eta'(\pi\pi\eta(\gamma\gamma))$	$1.40 \pm 0.25 \pm 0.07$	$1.37 \pm 0.26 \pm 0.08$	$1.34 \pm 0.27 \pm 0.11$	$1.30 \pm 0.50 \pm 0.12$
$D^0\eta'(\rho^0\gamma)$	$1.58 \pm 0.42 \pm 0.09$	$1.79 \pm 0.57 \pm 0.10$	$1.91 \pm 0.54 \pm 0.15$	$1.55 \pm 0.89 \pm 0.16$
$D^{*0}(D^0\pi^0)\pi^0$	$2.95 \pm 0.25 \pm 0.30$	$2.95 \pm 0.29 \pm 0.33$	$3.52 \pm 0.29 \pm 0.43$	$2.32 \pm 0.56 \pm 0.24$
$D^{*0}(D^0\gamma)\pi^0$	$3.49 \pm 0.40 \pm 0.83$	$2.25 \pm 0.50 \pm 0.63$	$3.02 \pm 0.50 \pm 0.90$	$3.53 \pm 1.14 \pm 0.99$
$D^{*0}(D^0\pi^0)\eta(\gamma\gamma)$	$2.52 \pm 0.32 \pm 0.26$	$2.57 \pm 0.33 \pm 0.29$	$2.41 \pm 0.32 \pm 0.32$	$4.09 \pm 0.74 \pm 0.49$
$D^{*0}(D^0\gamma)\eta(\gamma\gamma)$	$2.62 \pm 0.45 \pm 0.33$	$2.81 \pm 0.49 \pm 0.35$	$2.87 \pm 0.55 \pm 0.39$	$2.75 \pm 0.78 \pm 0.36$
$D^{*0}(D^0\pi^0)\eta(\pi\pi\pi^0)$	$2.27 \pm 0.50 \pm 0.20$	$2.60 \pm 0.55 \pm 0.24$	$1.93 \pm 0.46 \pm 0.22$	$1.21 \pm 0.87 \pm 0.13$
$D^{*0}(D^0\gamma)\eta(\pi\pi\pi^0)$	$2.93 \pm 0.71 \pm 0.32$	$2.55 \pm 0.80 \pm 0.29$	$1.94 \pm 0.81 \pm 0.24$	-
$D^{*0}(D^0\pi^0)\omega$	$5.07 \pm 0.45 \pm 0.47$	$4.00 \pm 0.49 \pm 0.36$	$4.38 \pm 0.51 \pm 0.51$	$5.02 \pm 0.98 \pm 0.53$
$D^{*0}(D^0\gamma)\omega$	$3.66 \pm 0.64 \pm 0.41$	$4.46 \pm 0.80 \pm 0.56$	$4.59 \pm 0.87 \pm 0.57$	$4.28 \pm 1.71 \pm 0.57$
$D^{*0}(D^0\pi^0)\eta'(\pi\pi\eta(\gamma\gamma))$	$1.09 \pm 0.38 \pm 0.09$	$1.67 \pm 0.44 \pm 0.15$	$1.34 \pm 0.49 \pm 0.15$	-
$D^{*0}(D^0\gamma)\eta'(\pi\pi\eta(\gamma\gamma))$	$0.75 \pm 0.49 \pm 0.24$	-	$1.19 \pm 0.69 \pm 0.39$	-
$D^{*0}(D^0\pi^0)\eta'(\rho^0\gamma)$	$2.10 \pm 0.82 \pm 0.23$	$1.21 \pm 0.90 \pm 0.14$	$1.45 \pm 0.95 \pm 0.18$	-
$D^{*0}(D^0\gamma)\eta'(\rho^0\gamma)$	-	-	-	-

the result from the MC simulation assuming the PDG branching ratios of $B^- \to D^{(*)0}\rho^-$ [25]).

to the result obtained when computing the expected signal yield in the case where the above relative PDF normalization ratio of the $B^- \to D^{(*)0}\rho^-$ backgrounds is fully computed from the MC simulation (*i.e.* when assuming the PDG branching fractions [25]).

The acceptance of $\overline{B}^0 \to D^{*0}\omega$ is estimated from the sum of purely longitudinally ($f_L = 0$) and transversally ($f_L = 1$) polarized MC simulation signals, weighted by our measurement of f_L (see Sec. VI). The systematic uncertainty in the fraction of $D^{*0}\omega$ longitudinal polarization is then estimated by varying f_L by $\pm 1\sigma$ in the estimation of the signal acceptance. This contribution is small and slightly more than 1%, while it would be estimated to be about 10.5% if the fraction f_L was unknown. This is one of the motivations for measuring the polarization of the channel $\overline{B}^0 \to D^{*0}\omega$ (see Sec. VI).

The most significant sources of systematic uncertainties come from the π^0/γ reconstruction, from the ΔE fits, and from the uncertainties on the known world average branching fractions of the secondary channels. In the case of the modes $\overline{B}^0 \to D^{(*)0}\pi^0$, the contributions from $B^- \to D^{(*)0}\rho^-$ backgrounds are also not negligible.

V. RESULTS FOR THE $\mathcal{B}$ MEASUREMENTS

The $\mathcal{B}$ measured in the different secondary decay channels reconstructed in this analysis are given in Table IV (for missing entries in the Table; see the discussion on discarded sub-modes in Sec. III D 6).

These $\mathcal{B}$ are combined using the so-called Best Linear Unbiased Estimate (*BLUE*) technique [34], that accounts for the correlation between the various modes. In the *BLUE* method the average value is a linear combination of the individual measurements:

$$\mathcal{B} = \sum_i (\alpha_i \times \mathcal{B}_i), \tag{13}$$

where each coefficient α_i is a constant weight, not necessarily positive, for a given measurement $\mathcal{B}_i$. The condition $\sum_i \alpha_i = 1$ ensures that the method is unbiased. The set of coefficients $\alpha = (\alpha_1,\ \alpha_2, ...)$ (a vector with t elements) is calculated so that the variance of $\mathcal{B}$ is minimal

$$\alpha = \frac{E^{-1}U}{U^T E^{-1} U}, \tag{14}$$

where U is a t-component vector with elements all equal to 1: $U = (1, 1, ...)$, U^T its transpose, and E is the $(t \times t)$ error matrix. The variance of $\mathcal{B}$ is then given by:

$$\sigma^2 = \alpha^T E \alpha. \tag{15}$$

The error matrix E is evaluated for each source of systematics. Its matrix elements are, for two modes i and j:

$$E_{ij} = \rho_{ij}\sigma_i\sigma_j, \tag{16}$$

where σ_i and σ_j are the uncertainties from the corresponding systematics for the modes i and j, and ρ_{ij} is their correlation coefficient. We distinguish several types of systematics according to their correlations between the modes:

TABLE V. Branching fractions of channels $\overline{B}^0 \to D^{(*)0}h^0$, where the $\mathcal{B}$ measured in each D^0 modes are combined. For the modes with $h^0 = \eta,\ \eta'$, we give the combination (comb.) of the $\mathcal{B}$ computed with each sub-modes of $\eta^{(\prime)}$. The first uncertainty is statistical and the second is systematics. The quality of the combination is given through the value of $\chi^2/ndof$, with the corresponding probability (p-value) given in parenthesis in percents.

$\overline{B}^0$ mode	$\mathcal{B}(\times 10^{-4})$	$\chi^2/ndof$ (p-value %)
$D^0\pi^0$	$2.69 \pm 0.09 \pm 0.13$	2.81/3 (42.2)
$D^0\eta(\gamma\gamma)$	$2.50 \pm 0.11 \pm 0.12$	0.45/3 (93.0)
$D^0\eta(\pi\pi\pi^0)$	$2.56 \pm 0.16 \pm 0.13$	0.39/3 (94.2)
$D^0\eta$ (comb.)	$2.53 \pm 0.09 \pm 0.11$	0.95/7 (99.6)
$D^0\omega$	$2.57 \pm 0.11 \pm 0.14$	3.19/3 (36.3)
$D^0\eta'(\pi\pi\eta(\gamma\gamma))$	$1.37 \pm 0.14 \pm 0.07$	0.05/3 (99.7)
$D^0\eta'(\rho^0\gamma)$	$1.73 \pm 0.28 \pm 0.08$	0.27/3 (96.6)
$D^0\eta'$ (comb.)	$1.48 \pm 0.13 \pm 0.07$	1.55/7 (98.1)
$D^{*0}\pi^0$	$3.05 \pm 0.14 \pm 0.28$	4.73/7 (69.3)
$D^{*0}\eta(\gamma\gamma)$	$2.77 \pm 0.16 \pm 0.25$	4.20/7 (75.6)
$D^{*0}\eta(\pi\pi\pi^0)$	$2.40 \pm 0.25 \pm 0.21$	3.81/6 (70.2)
$D^{*0}\eta$ (comb.)	$2.69 \pm 0.14 \pm 0.23$	10.48/14 (72.6)
$D^{*0}\omega$	$4.55 \pm 0.24 \pm 0.39$	4.05/7 (77.4)
$D^{*0}\eta'(\pi\pi\eta(\gamma\gamma))$	$1.37 \pm 0.23 \pm 0.13$	2.30/4 (68.1)
$D^{*0}(D^0\pi^0)\eta'(\rho^0\gamma)$	$1.81 \pm 0.42 \pm 0.16$	0.68/2 (71.2)
$D^{*0}\eta'$ (comb.)	$1.48 \pm 0.22 \pm 0.13$	3.78/7 (80.5)

- full correlation, $|\rho_{ij}| \sim 1$: neutrals (but uncertainties for π^0 and single γ are independent), PID, tracking, number of $B\overline{B}$, $\mathcal{B}(D^{*0})$, $D^{*0}\omega$ polarization in that mode,
- medium correlation: $\mathcal{B}(D^0)$, $\mathcal{B}(h^0)$, whose correlations are taken from the PDG [25] and range from 2% to 100%, $D^{(*)0}\rho^-$ background in $\overline{B}^0 \to D^{(*)0}\pi^0$,
- negligible correlation, $|\rho_{ij}| \sim 0$: statistical uncertainties, PDF systematics, selection on intermediate resonances, MC statistics.

The total error matrix E is then the sum of the error matrix for each source of uncertainty. The systematic (statistical) uncertainty on the combined value of $\mathcal{B}$ is computed by using Eq. (15) where the error matrix includes only the systematic (statistical) uncertainties.

The combined branching fractions in data are given in Table V with the χ^2 of the combinantion, the number of degrees of freedom of the combination ($ndof$), and the corresponding probability (p-value). The individual branching fractions together with the combined value are displayed in Figs. 5 and 6 and they are compared to the previous measurements by CLEO [8], *BABAR* [10, 14], and Belle [11, 12].

The results of this blind analysis, based on a data sample of 454×10^6 $B\overline{B}$ pairs, are fully compatible with our previous measurements [10, 14], and also with those of CLEO [8]. They are compatible with the measurements by Belle [11, 12] for most of the modes, except for $\overline{B}^0 \to D^{(*)0}\eta$, $D^{*0}\omega$, and $D^{*0}\pi^0$, where our results are larger.

As a cross check we also perform the $\mathcal{B}$ measurements with a sub-data set of only 88×10^6 $B\overline{B}$ pairs that we previously studied [10]. We found fully compatible $\mathcal{B}$ values with both statistical and systematic uncertainties lowered by significant amounts. In addition to a 5.1 times larger data set, with respect to 2004, we benefit from improved procedures to reconstruct and analyze the data collected by the *BABAR* detector . This updated analysis incorporates new decay modes, higher signal efficiency, better background rejection and treatment. It employs better fitting techniques and uses more sophisticated methods to combine the results obtained with the various sub-decay modes. We use additional control data samples and measure directly in the data the relative ratio of the $B^- \to D^{(*)0}\rho^-$ backgrounds.

These measurements are the most precise determinations of the $\mathcal{B}(\overline{B}^0 \to D^{(*)0}h^0)$ from a single experiment. They represent significant improvements with respect to the accuracy of the existing PDG averages [25].

VI. POLARIZATION OF $\overline{B}^0 \to D^{*0}\omega$

The polarization of the vector-vector (VV) decay $\overline{B}^0 \to D^{*0}\omega$ has never been measured. Until now, it was admitted to be similar to that of the decay $B^- \to D^{*0}\rho^-$, based on *Heavy Quark Effective Theory* (HQET) and factorization arguments [35]. The angular distributions for the decay $\overline{B}^0 \to D^{*0}\omega$ is described by three helicity amplitudes: the longitudinal H_0 amplitude and the transverse H_+ and H_- amplitudes. In the factorization description of $B \to VV$ decays, the longitudinal amplitude H_0 is expected to be dominant, leading to the fraction of longitudinal polarization, defined as:

$$f_L \equiv \frac{\Gamma_L}{\Gamma} = \frac{|H_0|^2}{|H_0|^2 + |H_+|^2 + |H_-|^2}, \qquad (17)$$

and predicted to be close to one [3, 36–38].

Significant transverse polarizations were measured in $B \to \phi K^*$ (see review in [25]) and investigated as possible signs of new physics [39], but could also be the result of non-factorizable QCD effects [40]. Similar effects were studied in the context of SCET [21], and are expected to arise in the $\overline{B}^0 \to D^{*0}\omega$ decay, in particular through enhanced electromagnetic penguin decays [41], leading to significative deviation of f_L from one. It has also been

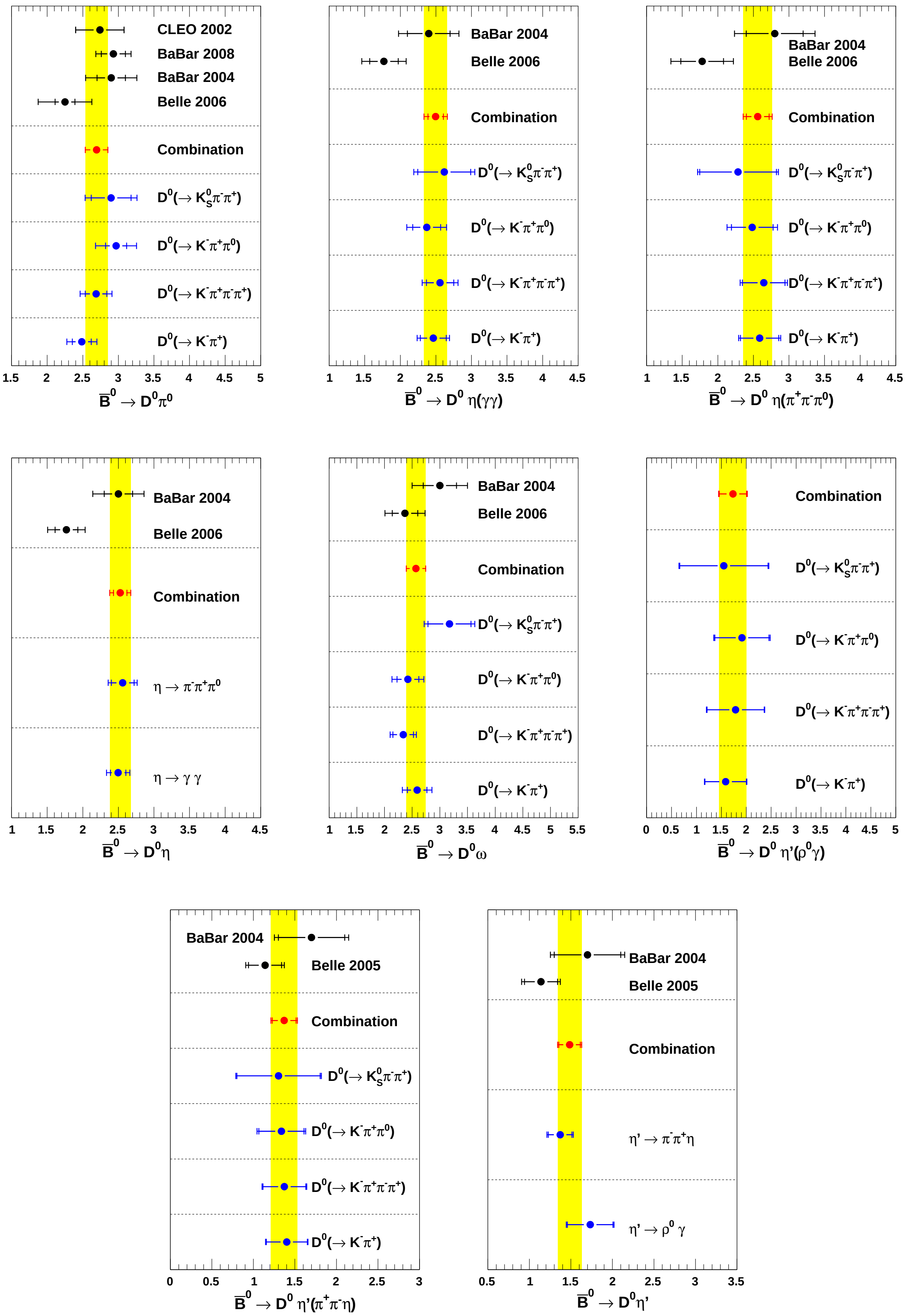

FIG. 5. $\mathcal{B}(\overline{B}^0 \to D^0 h^0)$ $(\times 10^{-4})$ for the individual reconstructed D^0 and h^0 channels (blue points) together with the *BLUE* combination (vertical yellow bands and the red points). The previous experimental results from *BABAR* [10, 14], Belle [11, 12], and CLEO [8] are also shown (black points). The uncertainty horizontal bars represent the statistical contribution alone and the quadratic sum of the statistical and systematic contributions. The width of the vertical yellow band corresponds to $\pm 1\sigma$ of the combined measurement, where the statistical and systematic uncertainties are summed in quadrature.

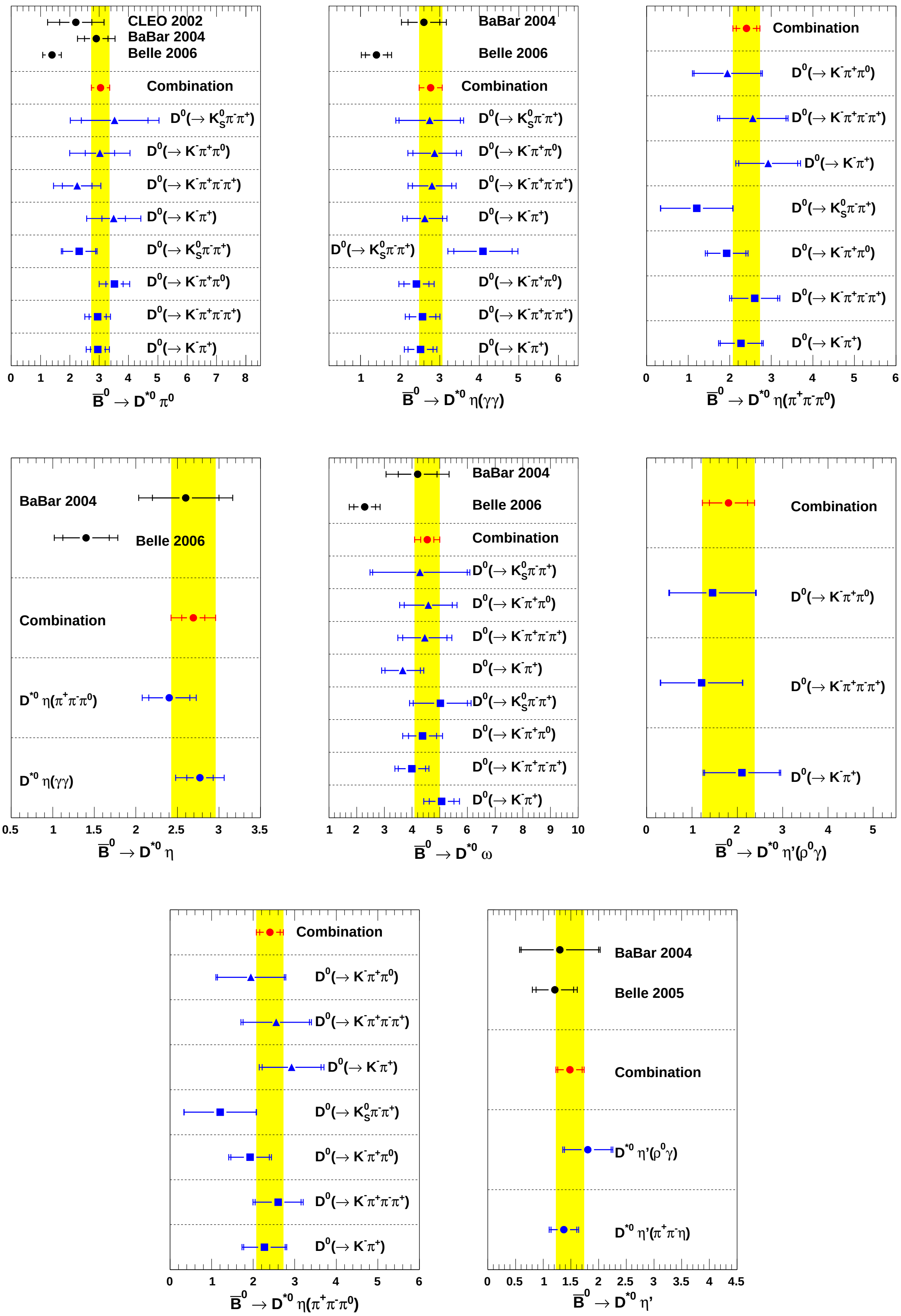

FIG. 6. $\mathcal{B}(\overline{B}^0 \to D^{*0}h^0)$ $(\times 10^{-4})$ for the individual reconstructed D^0, D^{*0}, and h^0 channels together with the *BLUE* combination (vertical yellow bands and the red points). The blue squares (triangles) are for measurements with the sub-decay $D^{*0} \to D^0\pi^0$ $(D^0\gamma)$. The previous experimental results from *BABAR* [10, 14], Belle [11, 12], and CLEO [8] are also shown (black points). The uncertainty horizontal bars represent the statistical contribution alone and the quadratic sum of the statistical and systematic contributions. The width of the vertical yellow band corresponds to $\pm 1\sigma$ of the combined measurement, where the statistical and systematic uncertainties are summed in quadrature.

argued in SCET studies that non-trivial long distance contributions to the $\overline{B}^0 \to D^{*0}\omega$ amplitude may allow a significant amount of transverse polarization of similar size to the longitudinal polarization, leading to a value $f_L \sim 0.5$.

Apart from the motivation of these phenomenological questions, the uncertainty on the angular polarization of $\overline{B}^0 \to D^{*0}\omega$ ($f_L \sim 0.5 - 1$) affects the kinematic acceptance of this channel and therefore would be the dominant contribution to the systematic effects for its $\mathcal{B}$ measurement. Hence we measure the fraction of longitudinal polarization for this decay mode. The analysis is performed with $\overline{B}^0 \to D^{*0}\omega$ candidates selected with the same requirements as for the $\mathcal{B}$ analysis described in the previous sections. We consider the sub-decays $D^{*0} \to D^0\pi^0$ and $D^0 \to K^-\pi^+$, $K^-\pi^+\pi^0$, $K^-\pi^+\pi^-\pi^+$, and $K^0_S\pi^+\pi^-$.

A. Description of the method

The differential decay rate of $\overline{B}^0 \to D^{*0}\omega$ for the subdecay $D^{*0} \to D^0\pi^0$ is [42]

$$\begin{aligned}\frac{d^3\Gamma}{d\cos(\theta_{D^*})d\cos(\theta_\omega)d\chi} \propto\ & 4|H_0|^2\cos^2(\theta_{D^*})\cos^2(\theta_\omega)+ \\ & \left[|H_+|^2+|H_-|^2+2(Re(H_+H_-^*)\cos(\chi)-Im(H_+H_-^*)\sin(2\chi))\right]\sin^2(\theta_{D^*})\sin^2(\theta_\omega)+ \\ & (Re(H_+H_0^*+H_-H_0^*)\cos(\chi)-Im(H_+H_0^*-H_-H_0^*)\sin(\chi))\sin(2\theta_{D^*})\sin(2\theta_\omega),\end{aligned} \tag{18}$$

where θ_{D^*} (θ_ω) is the helicity angle of the D^* (ω) meson (see Sec. III C 3 for definitions; for simpler notation we have replaced here θ_N by θ_ω). The angle χ, called the azimuthal angle, is the angle between the D^{*0} and ω decay planes in the $\overline{B}^0$ frame. Since the acceptance is nearly independent of χ, one can integrate over χ to obtain a simplified expression:

$$\begin{aligned}\frac{d^3\Gamma}{d\cos(\theta_{D^*})d\cos(\theta_\omega)} \propto\ & 4|H_0|^2\cos^2(\theta_{D^*})\cos^2(\theta_\omega)+ \\ & (|H_+|^2+|H_-|^2)\sin^2(\theta_{D^*})\sin^2(\theta_\omega).\end{aligned} \tag{19}$$

This differential decay width is proportional to

$$4f_L\cos^2(\theta_{D^*})\cos^2(\theta_\omega)+(1-f_L)\sin^2(\theta_{D^*})\sin^2(\theta_\omega), \tag{20}$$

which is the weighted sum of purely longitudinal ($f_L = 1$) and purely transverse ($f_L = 0$) contributions.

We employ high statistics MC simulations of exclusive signal samples of $\overline{B}^0 \to D^{*0}\omega$ decays with the two extreme configurations $f_L = 0$ and 1 to estimate the ratio of signal acceptance, $\varepsilon_0/\varepsilon_1$, of $f_L = 0$ events to $f_L = 1$ events. The longitudinal fraction f_L , can be expressed in terms of the fraction of background events, γ, and the fraction of $f_L = 1$ events in the observed data sample, α:

$$f_L = \frac{\alpha}{\alpha + (1-\alpha-\gamma)\cdot\frac{\varepsilon_0}{\varepsilon_1}}. \tag{21}$$

The fraction γ is taken from the fit of ΔE for a signal region $|\Delta E| < 2.5\sigma_{\Delta E}$ and $m_{\rm ES} > 5.27$ GeV/c^2, where $\sigma_{\Delta E}$ is the fitted ΔE width of the signal distribution, ranging from 20.8 to 23.3 MeV depending on the mode. The fraction α is determined from a simultaneous 2-dimensional fit to the distributions of the helicity angles $\cos(\theta_\omega)$ and $\cos(\theta_{D^*})$, for $\overline{B}^0 \to D^{*0}\omega$ candidates selected in the same signal region. The correlation between $\cos(\theta_\omega)$ and $\cos(\theta_{D^*})$ is found to be negligible.

The signal shapes are described with parabolas (see Eq. 20), except for the $\cos(\theta_\omega)$ distribution of $f_L = 0$ signal events, which is described by an MC simulation-based non-parametric PDF. It is for the following reason: the signal distribution of $\cos(\theta_\omega)$ is distorted around zero because of the selection cut on pion momentum and on the ω boost (see Sec. III B 3). The signal PDF parameters are fixed to those fitted on the $D^{*0}\omega$ simulations. The shape of the $\cos(\theta_\omega)$ and $\cos(\theta_{D^*})$ background distributions is taken from the data sideband $-280 < \Delta E < 280$ MeV and $5.235 < m_{\rm ES} < 5.27$ GeV/c^2. The consistency of the background shape was checked and validated for various regions of the sidebands in data and generic MC simulations. Possible biases on f_L from the fit are investigated with pseudo-experiment studies for various values of f_L. No significant biases are observed. An additional study is performed with embedded signal MC simulation, *i.e.* with signal events modeled from various different fully simulated signal samples. A small bias accounting for the description of the signal shape is observed and is corrected later on.

B. Statistical and systematic uncertainties

The statistical uncertainty on f_L is estimated with a conservative approach by varying independently the two fitted parameters α and γ by varying their values by $\pm1\sigma$ in Eq. (21). An extended study based on MC pseudo-experiments accounting correlations between α and γ gave slightly smaller uncertainty.

The uncertainty on the signal shape in the simultaneous 2-dimensional fit to $\cos(\theta_\omega)$ and $\cos(\theta_{D^*})$ is measured using the control sample $B^+ \to D^{*0}\pi^+$, with $D^{*0} \to D^0\pi^0$ and $D^0 \to K^-\pi^+$. This mode was chosen for its high purity and for its longitudinal fraction

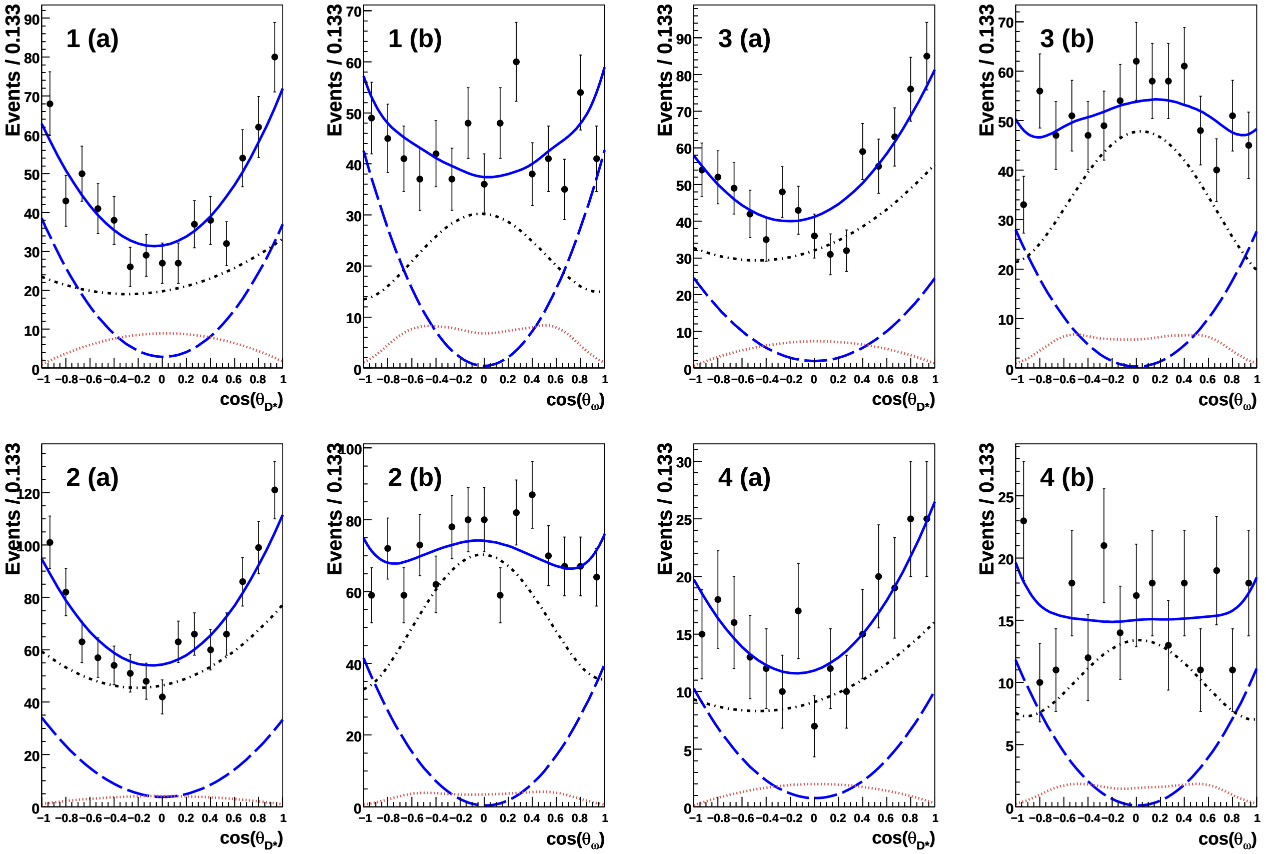

FIG. 7. Fitted distributions of the helicity $\cos(\theta_{D^*})$ (a) and $\cos(\theta_\omega)$ (b) in the channel $\overline{B}^0 \to D^{*0}\omega$ for the D^0 decay modes $K^-\pi^+$ (Fig. 1), $K^-\pi^+\pi^-\pi^+$ (Fig. 2), $K^-\pi^+\pi^0$ (Fig. 3) and $K^0_S\pi^+\pi^-$ (Fig. 4). The dots with error bars are data, the solid blue curve is the fitted total PDF, the dash-dot grey curve is the background contribution, the blue curve with long dash is the signal part with $f_L = 1$ and signal with $f_L = 0$ is the red curve with dots.

$f_L = 1$, which enables us to directly compare its shape to our signal $f_L = 1$. The distribution of the helicity angle of the D^{*0} is found to be wider in the data than in the MC, this difference being parameterized by a parabola. The uncertainty on the signal shape is then measured by refitting α, with the signal PDF being multiplied by the correction parabola. The relative difference is then taken as the uncertainty.

The uncertainty on the background shape is measured by refitting α with the background shape fitted in a lower data sideband $-280 < \Delta E < 280$ MeV and $5.20 < m_{\rm ES} < 5.235$ GeV/c^2. The relative difference is then taken as the uncertainty.

An uncertainty is assigned to the assumption of the acceptance being independent of χ. The acceptance of the MC signal is measured in bins of χ and fitted with a Fourier series to account for any deviation from flatness. The fitted function is then used as a parametrization of the acceptance dependency to χ in a study with pseudo-MC experiments and multiplied to the decay rate (see Eq. 18). Events are generated from this new decay rate and their $\cos(\theta_\omega) \times \cos(\theta_{D^*})$ distributions are fitted with the procedure described above. The small bias observed is assigned as a systematic uncertainty.

The uncertainty on the efficiency ratio $\varepsilon_0/\varepsilon_1$, from the limited amount of MC statistics available, is calculated assuming ε_0 and ε_1 to be uncorrelated, while the uncertainties on $\varepsilon_0/\varepsilon_1$ are calculated from the binomial distribution.

The various relative uncertainties are displayed in Table VI for the data and are found to be compatible with the ones calculated in MC simulations. The dominant uncertainty is statistical. Among the various systematics sources, the largest contribution comes from the signal parametrization.

As a check, the f_L measurement is applied in data first on the high purity and high statistics control sample $B^- \to D^{*0}\pi^-$, with $D^{*0} \to D^0\pi^0$ and $D^0 \to K^-\pi^+$. This channel is longitudinally polarized, *i.e.* $f_L = 1$. The fit of $\cos(\theta_{D^*})$ in data yields a value of f_L compatible with one, reinforcing the validity of the analysis procedure.

TABLE VI. Total relative uncertainties computed in data on the measurement of f_L in the channel $\overline{B}^0 \to D^{*0}\omega$, with $D^{*0} \to D^0\pi^0$ and $D^0 \to K^-\pi^+$, $K^-\pi^+\pi^0$, $K^-\pi^+\pi^-\pi^+$, and $K^0_S\pi^+\pi^-$.

Sources	$\Delta f_L/f_L$ (%)			
	$K\pi$	$K3\pi$	$K\pi\pi^0$	$K^0_S\pi\pi$
Signal PDFs	2.5	2.9	2.4	2.3
Bias	1.0	1.3	2.0	2.3
Background PDF	0.3	4.2	3.6	4.0
Limited MC statistics	0.1	0.2	0.3	0.3
Flat acceptance vs. χ	1.5	1.8	0.5	6.9
Total syst.	3.1	5.6	4.8	8.6
Statistical uncert.	9.6	16.3	16.3	25.6
Total uncert.	10.0	17.2	17.0	27.0

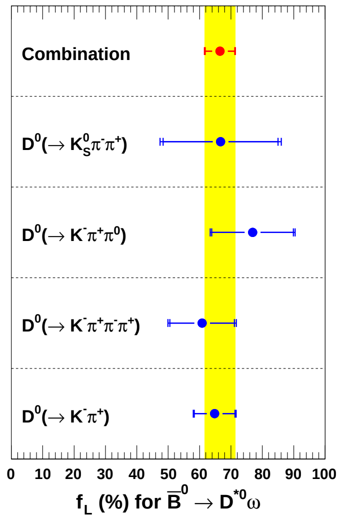

FIG. 8. Measurements of f_L with the four D^0 modes in data. The yellow band represents the *BLUE* combination.

C. Results for the fraction of longitudinal polarization f_L

The fitted data distributions of the cosine of the helicity angles are given in Fig. 7. The measurements for each D^0 channel are then combined with the *BLUE* statistical method [34] (see Sec. V) with $\chi^2/ndof = 1.01/3$ (*i.e.*: a probability of 79.9%), where $ndof$ is number of degrees of freedom. The measured values of f_L, α, γ and $\varepsilon_{00}/\varepsilon_{11}$ are given with the details of the combination in Table VII and in Fig. 8. The final result is $f_L = (66.5 \pm 4.7 \pm 1.5)\%$, where the first uncertainty is statistical and the second systematics. This is the first measurement of the longitudinal fraction of $\overline{B}^0 \to D^{*0}\omega$, with a relative precision of 7.4%.

TABLE VII. Values of α fitted in data, of the background fraction γ and of the acceptance ratio $\varepsilon_0/\varepsilon_1$, with the corresponding values of the longitudinal fraction f_L after the bias correction. The first quoted uncertainty is statistical and the second systematic.

D^0 mode	α (%)	γ (%)	$\varepsilon_0/\varepsilon_1$	f_L (%)
$K\pi$	33.4±2.7	52.0±1.9	1.093±0.012	64.8±6.5±2.1
$K3\pi$	18.8±2.3	71.2±2.5	1.068±0.017	60.8±10.3±3.6
$K\pi\pi^0$	19.6±2.1	76.0±2.3	1.109±0.021	76.9±13.0±3.8
$K^0_S\pi\pi$	24.9±4.2	66.0±4.9	1.092±0.016	66.7±18.3±6.2
Combi.		$f_L = (66.5 \pm 4.7 \pm 1.5)\%$		

This value differs significantly from the HQET prediction $f_L = (89.5 \pm 1.9)\%$ [35, 43]. This significant transverse amplitude in the $\overline{B}^0 \to D^{*0}\omega$ channel may arise from the same mechanism as the one responsible for the transverse polarization observed in $B \to \phi K^*$. It however supports the existence of effects from non trivial long distance contributions to the decay amplitude of $\overline{B}^0 \to D^{*0}\omega$ as predicted by SCET studies [21].

VII. DISCUSSION

A. Isospin analysis

The isospin symmetry relates the amplitudes of the decays $B^- \to D^{(*)0}\pi^-$, $\overline{B}^0 \to D^{(*)+}\pi^-$ and $\overline{B}^0 \to D^{(*)0}\pi^0$, which can be written as linear combinations of the isospin eigenstates $\mathcal{A}_{I,D^{(*)}}$, $I = 1/2,\ 3/2$ [5, 44]:

$$\begin{aligned} \mathcal{A}(D^{(*)0}\pi^-) &= \sqrt{3}\mathcal{A}_{3/2,D^{(*)}}, \\ \mathcal{A}(D^{(*)+}\pi^-) &= 1/\sqrt{3}\mathcal{A}_{3/2,D^{(*)}} + \sqrt{2/3}\mathcal{A}_{1/2,D^{(*)}}, \\ \mathcal{A}(D^{(*)0}\pi^0) &= \sqrt{2/3}\mathcal{A}_{3/2,D^{(*)}} - \sqrt{1/3}\mathcal{A}_{1/2,D^{(*)}}, \end{aligned} \tag{22}$$

leading to:

$$\mathcal{A}(D^{(*)0}\pi^-) = \mathcal{A}(D^{(*)+}\pi^-) + \sqrt{2}\mathcal{A}(D^{(*)0}\pi^0). \tag{23}$$

The relative strong phase between the eigenstates $\mathcal{A}_{1/2,D^{(*)}}$ and $\mathcal{A}_{3/2,D^{(*)}}$ is denoted as δ for the $D\pi$ system and δ^* for $D^*\pi$ system. Final state interactions between the states $D^{(*)0}\pi^0$ and $D^{(*)+}\pi^-$ may lead to a value of $\delta^{(*)}$ different from zero and, through constructive interference, to a larger value of $\mathcal{B}$ for $D^{(*)0}\pi^0$ than prediction obtained within the factorization approximation. One can also define the amplitude ratio $R^{(*)}$:

$$R^{(*)} = \frac{|\mathcal{A}_{1/2,D^{(*)}}|}{\sqrt{2}|\mathcal{A}_{3/2,D^{(*)}}|}. \quad (24)$$

In the heavy-quark limit, the factorization model predicts [45, 46] $\delta^{(*)} = \mathcal{O}(\Lambda_{\mathrm{QCD}}/m_b)$ and $R^{(*)} = 1 + \mathcal{O}(\Lambda_{\mathrm{QCD}}/m_b)$, where m_b represents the b quark mass and where the correction to "1" is also suppressed by a power of $1/N_c$, with N_c the number of colors. While SCET [19–21] predicts that the strong phases $\delta^{(*)}$ ($R^{(*)}$) have the same value in the $D\pi$ and $D^*\pi$ systems and significantly differ from 0 (1).

The strong phase $\delta^{(*)}$ can be computed with an isospin analysis of the $D^{(*)}\pi$ system. We use the world average values provided by the PDG [25] for $\mathcal{B}(B^- \to D^{(*)0}\pi^-)$, $\mathcal{B}(\overline{B}^0 \to D^{(*)+}\pi^-)$ values and for the B lifetime ratio $\tau(B^+)/\tau(B^0)$. The values of $\mathcal{B}(\overline{B}^0 \to D^{(*)0}\pi^0)$ are taken from this analysis. We calculate the values of $\delta^{(*)}$ and $R^{(*)}$ using a frequentist approach [47]:

$$\delta = (29.0^{+2.1}_{-2.6})^\circ, \quad R = \left(69.2^{+3.8}_{-3.9}\right)\%, \quad (25)$$

for $D\pi$ final states, and

$$\delta^* = (29.5^{+3.5}_{-4.5})^\circ, \quad R^* = \left(67.0^{+4.8}_{-4.7}\right)\%, \quad (26)$$

for $D^*\pi$ final states.

In both $D\pi$ and $D^*\pi$ cases, the amplitude ratio is significantly different from the factorization prediction $R^{(*)} = 1$. The strong phases are also significantly different from zero and are equal in the two systems $D\pi$ and $D^*\pi$ (0° is respectively excluded at 99.998% and 99.750% of confidence level), which points out that non-factorizable FSI are indeed not negligible. Those results confirm the SCET predictions.

B. Comparison to theoretical predictions on $\mathcal{B}(\overline{B}^0 \to D^{(*)0}h^0)$

Table VIII compares the $\mathcal{B}(\overline{B}^0 \to D^{(*)0}h^0)$ measured with this analysis to the predictions by factorization [3, 15, 48, 49] and pQCD [17, 18]. We confirm the conclusion by the previous *BABAR* analysis [10]: the values measured are higher by a factor of about three to five than the values predicted by factorization. The pQCD predictions are closer to experimental values but globally higher, except for the $D^{(*)0}\pi^0$ modes.

The ratios of the $\mathcal{B}$ are given in Table IX. It should be noted that the values of those ratios are not computed directly from those quoted in Table V, as we take advantage of the fact that common systematic uncertainties cancel between D^0h^0 and $D^{*0}h^0$ modes. Therefore the ratios of the $\mathcal{B}$ are first calculated for each sub-decays of D^0 and h^0, and then after combined with the BLUE method. The ratios $\mathcal{B}(\overline{B}^0 \to D^{*0}h^0)/\mathcal{B}(\overline{B}^0 \to D^0h^0)$ for $h^0 = \pi^0$, η, and η' are compatible with 1. Both are displayed in Fig. 9 together with the theoretical predictions.

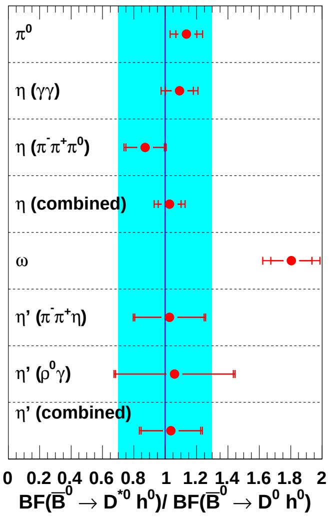

FIG. 9. Combined ratios $\mathcal{B}(\overline{B}^0 \to D^{*0}h^0)/\mathcal{B}(\overline{B}^0 \to D^0h^0)$ measured in this paper compared to theoretical prediction by SCET [21] (vertical solid line). The vertical band represent the estimated theoretical uncertainty from SCET.

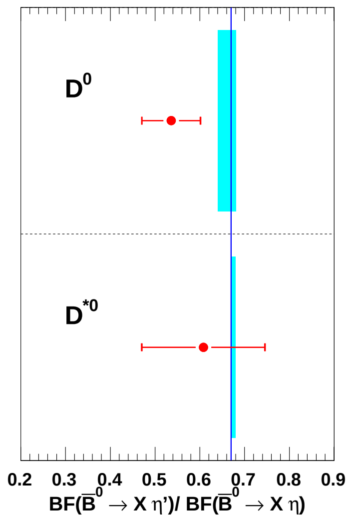

FIG. 10. Combined ratios $\mathcal{B}(\overline{B}^0 \to D^{*0}\eta')/\mathcal{B}(\overline{B}^0 \to D^{*0}\eta)$ and $\mathcal{B}(\overline{B}^0 \to D^0\eta')/\mathcal{B}(\overline{B}^0 \to D^0\eta)$ measured in this paper compared to theoretical prediction by SCET [21] (vertical line) and from factorization [48] (vertical bands).

Factorization predicts the ratio $\mathcal{B}(\overline{B}^0 \to D^{(*)0}\eta')/\mathcal{B}(\overline{B}^0 \to D^{(*)0}\eta)$ to have a value between 0.64 and 0.68 [48], related to the $\eta - \eta'$ mixing. Those ratios are also given in Table IX and Fig. 10 compares the theoretical predictions with our experimental measurements. The measured ratios are smaller than the predictions and are compatible at the level of less than

TABLE VIII. Comparison of the measured branching fraction $\mathcal{B}$, with the predictions by factorization [3, 15, 48, 49] and pQCD [17, 18]. The first quoted uncertainty is statistical and the second is systematic.

$\mathcal{B}(\overline{B}^0 \to)$ $(\times 10^{-4})$	This measurement	Factorization	pQCD
$D^0\pi^0$	$2.69 \pm 0.09 \pm 0.13$	0.58 [15]; 0.70 [3]	2.3-2.6
$D^{*0}\pi^0$	$3.05 \pm 0.14 \pm 0.28$	0.65 [15]; 1.00 [3]	2.7-2.9
$D^0\eta$	$2.53 \pm 0.09 \pm 0.11$	0.34 [15]; 0.50 [3]	2.4-3.2
$D^{*0}\eta$	$2.69 \pm 0.14 \pm 0.23$	0.60 [3]	2.8-3.8
$D^0\omega$	$2.57 \pm 0.11 \pm 0.14$	0.66 [15]; 0.70 [3]	5.0-5.6
$D^{*0}\omega$	$4.55 \pm 0.24 \pm 0.39$	1.70 [3]	4.9-5.8
$D^0\eta'$	$1.48 \pm 0.13 \pm 0.07$	0.30-0.32 [49]; 1.70-3.30 [48]	1.7-2.6
$D^{*0}\eta'$	$1.48 \pm 0.22 \pm 0.13$	0.41-0.47 [48]	2.0-3.2

two σ.

The SCET [19–21] does not predict the absolute value of the $\mathcal{B}$ but it predicts that the ratios $\mathcal{B}(\overline{B}^0 \to D^{*0}h^0)/\mathcal{B}(\overline{B}^0 \to D^0h^0)$ are about equal to one for $h^0 = \pi^0$, η and η'. For $h^0 = \omega$ that prediction holds only for the longitudinal component of $\overline{B}^0 \to D^{*0}\omega$, as non trivial long-distance QCD interactions may increase the transverse amplitude. We measure the fraction of longitudinal polarization to be $f_L = (66.5 \pm 4.7(\text{stat.}) \pm 1.5(\text{syst.}))\%$ in the decay mode $\overline{B}^0 \to D^{*0}\omega$, and find that the ratio $\mathcal{B}(\overline{B}^0 \to D^{*0}\omega)/\mathcal{B}(\overline{B}^0 \to D^0\omega)$ is significantly higher than one, as expected by SCET [21]. The SCET gives also a prediction about the ratio $\mathcal{B}(\overline{B}^0 \to D^{(*)0}\eta')/\mathcal{B}(\overline{B}^0 \to D^{(*)0}\eta) \simeq 0.67$, which is similar to the prediction by factorization.

TABLE IX. Ratios of branching fractions $\mathcal{B}(\overline{B}^0 \to D^{*0}h^0)/\mathcal{B}(\overline{B}^0 \to D^0h^0)$ and $\mathcal{B}(\overline{B}^0 \to D^{(*)0}\eta')/\mathcal{B}(\overline{B}^0 \to D^{(*)0}\eta)$. The first uncertainty is statistical, the second is systematic.

$\mathcal{B}$ ratio	This measurement
$D^{*0}\pi^0/D^0\pi^0$	$1.14 \pm 0.07 \pm 0.08$
$D^{*0}\eta(\gamma\gamma)/D^0\eta(\gamma\gamma)$	$1.09 \pm 0.09 \pm 0.08$
$D^{*0}\eta(\pi\pi\pi^0)/D^0\eta(\pi\pi\pi^0)$	$0.87 \pm 0.12 \pm 0.05$
$D^{*0}\eta/D^0\eta$ (Combined)	$1.03 \pm 0.07 \pm 0.07$
$D^{*0}\omega/D^0\omega$	$1.80 \pm 0.13 \pm 0.13$
$D^{*0}\eta'(\pi\pi\eta)/D^0\eta'(\pi\pi\eta)$	$1.03 \pm 0.22 \pm 0.07$
$D^{*0}\eta'(\rho^0\gamma)/D^0\eta'(\rho^0\gamma)$	$1.06 \pm 0.38 \pm 0.09$
$D^{*0}\eta'/D^0\eta'$ (Combined)	$1.04 \pm 0.19 \pm 0.07$
$D^0\eta'/D^0\eta$	$0.54 \pm 0.07 \pm 0.01$
$D^{*0}\eta'/D^{*0}\eta$	$0.61 \pm 0.14 \pm 0.02$

VIII. CONCLUSIONS

We measure the branching fractions of the color-suppressed decays $\overline{B}^0 \to D^{(*)0}h^0$, where $h^0 = \pi^0$, η, ω, and η' with $454\times10^6 B\overline{B}$ pairs. All the measurements are mostly in agreement with the previous results [8, 10–12, 14] and are the most precise determinations of the $\mathcal{B}(\overline{B}^0 \to D^{(*)0}h^0)$ from a single experiment. They represent significant improvements with respect to the accuracy of the existing PDG averages [25].

For the first time we also measure the fraction of longitudinal polarization f_L in the decay mode $\overline{B}^0 \to D^{*0}\omega$ to be significantly smaller than 1, and equal to $(66.5 \pm 4.7(\text{stat.}) \pm 1.5(\text{syst.}))\%$. This reinforces the conclusion drawn from the $\mathcal{B}$ measurements on the validity of factorisation in color-suppressed decays and supports expectations from SCET.

We confirm the significant differences from theoretical predictions by factorization and provide strong constraints on the models of color-suppressed decays. In particular our results support most of the predictions of SCET on $\overline{B}^0 \to D^{(*)0}h^0$ [19–21].

IX. ACKNOWLEDGMENTS

We are grateful for the extraordinary contributions of our PEP-II colleagues in achieving the excellent luminosity and machine conditions that have made this work possible. The success of this project also relies critically on the expertise and dedication of the computing organizations that support *BABAR*. The collaborating institutions wish to thank SLAC for its support and the kind hospitality extended to them. This work is supported by the US Department of Energy and National Science Foundation, the Natural Sciences and Engineering Research Council (Canada), the Commissariat à l'Energie Atomique and Institut National de Physique Nucléaire et de Physique des Particules (France), the Bundesministerium für Bildung und Forschung and Deutsche Forschungsgemeinschaft (Germany), the Istituto Nazionale di Fisica Nucleare (Italy), the Foundation for Fundamental Research on Matter (The Netherlands), the Research Council of Norway, the Ministry of Education and Science of the Russian Federation, Ministerio de Ciencia e Innovación (Spain), and the Science and Technology Facilities Council (United Kingdom). Individuals have received support from the Marie-Curie IEF program (European Union), the A. P. Sloan Foundation (USA) and the Binational Science Foundation (USA-Israel).

---

[1] H-Y. Cheng, C-K. Chua, and A. Soni, Phys. Rev. D **71**, 014030 (2005).
[2] D. Du, Phys. Lett. B **406**, 110 (1997).
[3] M. Neubert and B. Stech, in *Heavy Flavours II*, eds. A.J. Buras and M. Lindner (World Scientific, Singapore, 1998), p. 294.
[4] M. Bauer, B. Stech and M. Wirbel, Z. Phys. C **34**, 103 (1987).
[5] M. Neubert and A.A. Petrov, Phys. Lett. B **519**, 50 (2001).
[6] A. Deandrea, N. Di Bartolomeo, R. Gatto, and G. Nardulli, Phys. Lett. B **318**, 549 (1993); A. Deandrea *et al.*, *ibid.* **320**, 170 (1994).
[7] K. Honscheid, K. R. Schubert, and R. Waldi, Z. Phys. C **63**, 117 (1994).
[8] T. E. Coan *et al.* (CLEO Collaboration), Phys. Rev. Lett. **88**, 062001 (2002).
[9] K. Abe *et al.* (Belle Collaboration), Phys. Rev. Lett. **88**, 052002 (2002).
[10] B. Aubert *et al.* (*BABAR* Collaboration), Phys. Rev. D **69**, 032004 (2004).
[11] J. Schümann *et al.* (Belle Collaboration), Phys. Rev. D **72**, 011103 (2005).
[12] S. Blyth *et al.* (Belle Collaboration), Phys. Rev. D **74**, 092002 (2006).
[13] A. Kuzmin *et al.* (Belle Collaboration), Phys. Rev. D **76**, 012006 (2007).
[14] B. Aubert *et al.* (*BABAR* Collaboration), Phys. Rev. D **78**, 052005 (2008).
[15] C-K. Chua, W-S. Hou, and K-C. Yang, Phys. Rev. D **65**, 096007 (2002).
[16] L.E. Leganger and J.O. Eeg, Phys. Rev. D **82**, 074007 (2010).
[17] Y.Y Keum, T. Kurimoto, H. Li, C.D Lü and A.I. Sanda, Phys. Rev. D **69**, 094018 (2004).
[18] C.D Lü, Phys. Rev. D **68**, 097502 (2003).
[19] C.W. Bauer, D. Pirjol and I.W. Stewart, Phys. Rev. D **65**, 054022 (2002).
[20] S. Mantry, D. Pirjol, and I.W. Stewart, Phys. Rev. D **68** 114009 (2003).
[21] A.E. Blechman, S. Mantry, and I.W. Stewart, Phys. Lett. B **608**, 77 (2005).
[22] C-K. Chua and W-S. Hou, Phys. Rev. D **77**, 116001 (2008). R. Fleischer, N. Serra, and N. Tuning, Phys. Rev. D **83**, 014017 (2011).
[23] M. Gronau, Phys. Lett. B **557**, 198 (2003). M. Gronau, Y. Grossman, N. Shuhmaher, A. Soffer, and J. Zupan, Phys. Rev. D **69** 113003 (2004). R. Fleischer, Phys. Lett. B **562**, 234 (2003) and Nucl. Phys. B **659**, 321 (2003). B. Aubert *et al.* (*BABAR* Collaboration), Phys. Rev. Lett. **99**, 081801 (2007).
[24] B. Aubert *et al.* (*BABAR* Collaboration), Nucl. Instrum. Methods Phys. Res., Sect. A **479**, 1 (2002).
[25] K. Nakamura *et al.*(Particle Data Group), J. Phys. G **37**, 075021 (2010).
[26] D. Lange, Nucl. Instrum. Methods Phys. Res., Sect. A **462**, 152 (2001).
[27] T. Sjöstrand, S. Mrenna and P. Skands, Comput. Phys. Commun. **178**, 852 (2008).
[28] T. Sjöstrand, Comput. Phys. Commun. **82**, 74 (1994).
[29] S. Agostinelli *et al.* (Geant4 Collaboration), Nucl. Instrum. Methods Phys. Res., Sect. A **506**, 250 (2003).
[30] The so called empirically modified Novosibirsk function divides the fitting region into a peaking region, a low tail region and a high tail region. For a variable x, the modified Novosibirsk function $f(x) = A_p \times \exp(g(x))$, where $g(x)$ is defined, in the peak region $x_1 < x < x_2$, as

$$-\ln 2 \times \left(\frac{\ln\left(1 + 2\tau\sqrt{\tau^2+1}\frac{x-x_p}{\sigma_p\sqrt{2\ln 2}}\right)}{\ln(1+2\tau^2 - 2\tau\sqrt{\tau^2+1})} \right)^2 ,$$

in the low tail region $x < x_1$, as

$$\frac{\tau\sqrt{\tau^2+1}(x-x_1)\sqrt{2\ln 2}}{\sigma_p(\sqrt{\tau^2+1}-\tau)^2 \ln(\sqrt{\tau^2+1}+\tau)} + \rho_1 \left(\frac{x-x_1}{x_p-x_1}\right)^2 - \ln 2,$$

and in the high tail region $x > x_2$, as

$$-\frac{\tau\sqrt{\tau^2+1}(x-x_2)\sqrt{2\ln 2}}{\sigma_p(\sqrt{\tau^2+1}+\tau)^2 \ln(\sqrt{\tau^2+1}+\tau)} + \rho_2 \left(\frac{x-x_2}{x_p-x_2}\right)^2 - \ln 2.$$

The parameters are:

- A_p is the value at the maximum of the function,
- x_p is the peak position,
- σ_p is the width of the peak defined as the width at half-height divided by $2\sqrt{2\ln 2} \simeq 2.35$,
- ξ is an asymmetry parameter.

The positions $x_{1,2}$ are $x_p + \sigma_p\sqrt{2\ln 2}\left(\frac{\xi}{\sqrt{\xi^2+1}} \mp 1\right)$.
[31] J.C. Anjos *et al.* (E691 Collaboration), Phys. Rev. D **48**, 56 (1993).
[32] A. Höcker *et al.* (TMVA Group), CERN Report No. CERN-OPEN-2007-007 (2007).
[33] S.M. Berman and M. Jacob, Phys. Rev. Lett. **139**, 1023 (1965).
[34] L. Lyons, D. Gibaut, and P. Clifford, Nucl. Instrum. Methods Phys. Res., Sect. A **270** 110 (1988). B. Aubert *et al.* (*BABAR* Collaboration), Phys. Rev. D **78**, 112003 (2008).
[35] S.E. Csorna *et al.* (CLEO Collaboration), Phys. Rev. D **67**, 112002 (2003).
[36] A.R. Williamson, *Proccedings of the conference FPCP06*, hep-ph/0605196 (2006).
[37] J.G. Koerner and G.R. Goldstein, Phys. Lett. B **89**, 105 (1979).

[38] B. Aubert *et al.* (*BABAR* Collaboration), Phys. Rev. Lett. **92**, 141801 (2004).

[39] P.K. Das and K.C. Yang, Phys. Rev. D **71**, 094002 (2005). Y.D. Yang, R. Wang and G.R. Lu, Phys. Rev. D **72**, 015009 (2005). C.S. Huang, P. Ko, X.H. Wu, and Y.D. Yang, Phys. Rev. D **73**, 034026 (2006). B. Aubert *et al.* (*BABAR* Collaboration), Phys. Rev. D **78**, 092008 (2008).

[40] H.Y. Cheng, C.K. Chua, and A. Soni, Phys. Rev. D **71**, 014030 (2005).

[41] M. Beneke, J. Rohrer, and D. Yang, Phys. Rev. Lett. **96**, 141801 (2006).

[42] G. Kramer and W.F. Palmer, Phys. Rev. D **45**, 193216 (1992).

[43] J.L. Rosner, Phys. Rev. D **42**, 3732 (1990). M. Neubert, Phys. Lett. B **264**, 455 (1991). G. Kramer, T. Mannel and W.F. Palmer, Z. Phys. C **55**, 497 (1992). J.D. Richman, *Heavy Quark and CP Violation, in Probing the Standard Model of Particle Interactions*, Les Houches Session LXVIII, 1997 (Elsevier, Amsterdam, 1999), eds. R. Gupta, A. Morel, E. De Rafael, and F. David.

[44] J.L. Rosner, Phys. Rev. D **60**, 074028 (1999).

[45] M. Beneke, G. Buchalla, M. Neubert, and C.T. Sachrajda, Nucl. Phys. B **591**, 313 (2000).

[46] H-Y. Cheng and K-C Yang, Phys. Rev. D **59**, 092004 (1999).

[47] J. Charles *et al.* (CKMfitter group), Eur. Phys. Jour. C **41**, 1-131 (2005).

[48] A. Deandrea and A.D. Polosa, Eur. Phys. Jour. **22**, 677 (2002).

[49] J.O. Eeg, A. Hiorth, and A.D. Polosa, Phys. Rev. D **65**, 054030 (2002).